Title: Aging-related inflammation driven by cellular senescence enhances NAD consumption via activation of CD38^{+} macrophages

Authors: Anthony J. Covarrubias[1,2], Jose Alberto Lopez-Dominguez†[1], Rosalba Perrone†[1], Abhijit Kale†[1], John Newman[1,2], Shankar S. Iyer[4], Mark S. Schmidt[6], Herbert G. Kasler[1], Kyong-Oh Shin[7], Yong-Moon Lee[7], Issam Ben-Sahra[5], Melanie Ott[3], Charles Brenner[6], Judith Campisi[1], Eric Verdin[1,2,] *.

Affiliations:
†Authors Contributed Equally
[1]Buck Institute for Research on Aging, Novato, CA 94945, USA
[2]UCSF Department of Medicine, San Francisco, CA 94158, USA
[3]Gladstone Institutes, Virology and Immunology, San Francisco, CA 94158, USA
[4]Division of Gastroenterology, Hepatology and Endoscopy, Department of Medicine, Brigham and Women's Hospital, Harvard Medical School, Boston, MA 02115, USA
[5]Department of Biochemistry and Molecular Genetics, Northwestern University, Chicago, IL 60607, USA
[6]Department of Biochemistry, Carver College of Medicine, University of Iowa, Iowa City, IA 52242, USA
[7]College of Pharmacy, Chungbuk National University, Cheongju 28644, Republic of Korea Kyong-Oh Shin, current address: Department of Food Science and Nutrition, Hallym University, Chuncheon 24252, Republic of Korea

***Corresponding author:**
Eric Verdin
Buck Institute for Research on Aging
8001 Redwood Blvd.
Novato, CA 94945
Email: everdin@buckinstitute.org
Phone: 415-209-2250

Summary:
Decline in tissue NAD levels during aging has been linked to aging-associated diseases, such as age-related metabolic disease, physical decline, and Alzheimer's disease. However, the mechanism for aging-associated NAD decline remains unclear. Here we report that pro-inflammatory M1 macrophages, but not naïve or M2 macrophages, highly express the NAD consuming enzyme CD38 and have enhanced CD38-dependent NADase activity. Furthermore, we show that aging is associated with enhanced inflammation due to increased senescent cells, and the accumulation of CD38 positive M1 macrophages in visceral white adipose tissue. We also find that inflammatory cytokines found in the supernatant from senescent cells (Senescence associated secretory proteins, SASP) induces macrophages to proliferate and express CD38. As senescent cells progressively accumulate in adipose tissue during aging, these results highlight a new causal link between visceral tissue senescence and tissue NAD

decline during aging and may present a novel therapeutic opportunity to maintain NAD levels during aging.

Keywords: NAD metabolism, CD38, Aging, Inflammation, Macrophages, Senescent cells, Senescence associated secretory phenotype (SASP), Macrophage polarization**,** NAMPT

Introduction:

Nicotinamide adenine dinucleotide (NAD) is a redox coenzyme central to energy metabolism and an essential cofactor for non-redox NAD dependent enzymes including sirtuins and poly-ADP-ribose polymerases (PARPs) (Canto et al., 2015). NAD, first termed "cozymase," was found to boost the cell-free glucose fermentation rate of yeast extracts (Harden, 1906). Early in the 20th century, NAD deficiency was linked to pellagra, a disease characterized by dermatitis, diarrhea, dementia, and eventually death (Belenky et al., 2007). More recently, a progressive decrease in NAD levels during aging in both rodents and humans has been documented in multiple tissues including the liver, adipose tissue, and muscle (Yoshino et al., 2018). Remarkably, restoration of NAD levels with the NAD precursor vitamins nicotinamide riboside (NR), nicotinamide (NAM) and nicotinic acid (NA), in addition to the biosynthetic NAD precursor nicotinamide mononucleotide (NMN) appear to mitigate aging-associated diseases (Mitchell et al., 2018; Verdin, 2015; Yoshino et al., 2018). These observations have stimulated a flurry of research activity aiming to better understand how NAD levels affect the aging process and how or why NAD levels decline during aging, with the goal of developing therapeutics to combat aging-related disease.

NAD can be synthesized from tryptophan through the *de novo* pathway and by salvage of either of the three NAD precursor vitamins (Verdin, 2015). While dietary precursors can contribute to NAD pools in a manner that depends on which pathways are expressed in particular tissues (Bogan and Brenner, 2008), the prevailing thought is that the recycling of NAM via nicotinamide phosphoribosyltransferase (NAMPT) is the predominant metabolic pathway most cells use to maintain intracellular NAD levels (Liu et al., 2018). The rate of NAD synthesis is countered by the rate of consumption by NAD consuming enzymes including sirtuins, PARPs, and the CD38 and CD157 NAD hydrolases. As NAD levels decrease, a key unanswered question in the field is whether this results from reduced de novo NAD biosynthesis, reduced NAM salvage, enhanced NAD consumption, or a combination of these effects either as a function of age or episodes of metabolic imbalance.

There is evidence of reduced NAM salvage as aging-associated inflammation leads to reduced expression of NAMPT (Yoshino et al., 2011). Thus, reduced NAMPT protein levels may contribute to declining NAD levels. There is also evidence for increased expression of key NAD consuming enzymes such as PARPs and CD38 during aging (Mouchiroud et al., 2013). PARPs, in particular the ubiquitously expressed PARP1 and PARP2, are activated as a result of DNA damage during aging (Lopez-Otin et al., 2013). Defective DNA repair mechanisms are associated with increased PARP activation and progeroid (premature aging) diseases such as Cockayne syndrome and Werner's disease (Kim et al., 2005; Li et al., 2004; Scheibye-Knudsen et al., 2014).

However, it has recently been reported that PARP expression decreases during aging concomitant with increased expression of CD38, a transmembrane protein that consumes NAD to form cyclic ADP-ribose (cADPR), ADP-ribose (ADPR) and NAM (Camacho-Pereira et al., 2016). *Cd38 KO* mice were protected from age-related NAD decline and had enhanced metabolic health as a result of increased NAD levels and SIRT3 dependent mitochondrial function, suggesting that CD38 is the primary NAD-consuming enzyme in age-related NAD decline (Camacho-Pereira et al., 2016). However, these data do not address which cells express CD38 in aged tissues and what mechanism(s) drive aberrant CD38 expression during the process of aging and/or episodes of metabolic stress.

CD38 is ubiquitously expressed by immune cells and was first identified as a T cell activation marker (Quarona et al., 2013; Reinherz et al., 1980). Its expression increases during inflammatory conditions including colitis, sepsis, and HIV infection (Jackson and Bell, 1990; Savarino et al., 2000; Schneider et al., 2015). Chronic low grade inflammation during aging, termed “inflammaging” (Franceschi et al., 2000), is a leading mechanism of aging-associated diseases and has been described as a significant risk factor for morbidity and mortality (Franceschi and Campisi, 2014). Sustained activation of the immune system is energetically costly and requires sufficient amounts of metabolites to fuel effector functions (Ganeshan and Chawla, 2014). Thus, the immune system and metabolism are highly integrated. Despite this knowledge, it is unclear how age-related inflammation affects NAD metabolism and the aging process.

To study possible links between age-associated NAD decline and inflammation, we focused on visceral adipose tissue. By studying this tissue during the switch from lean to obese conditions much has been learned regarding how inflammation influences metabolic homeostasis, and how nutrient status in turn influences immunity (Hotamisligil, 2017). As obesity develops, peripheral monocytes are recruited to adipose tissue by adipokines, leading to a progressive infiltration of pro-inflammatory M1-like macrophages, and the displacement of anti-inflammatory resident M2 macrophages (Lumeng et al., 2007; Weisberg et al., 2003; Xu et al., 2003). Increased M1-like macrophages promote a pro-inflammatory state accompanied by insulin resistance, reduced rates of lipolysis, reduced tissue homeostasis, and the recruitment of macrophages to dying or stressed adipocytes resulting in the formation of “crown like structures” (Murano et al., 2008; Sica and Mantovani, 2012). This model suggests that macrophages, which are found in high abundance in key metabolic tissues such as liver and adipose tissue, may regulate metabolic health and disease through M1/M2 polarization and inflammatory signaling. We hypothesized that expression of NAD consuming enzymes including CD38 by adipose tissue macrophages contributes to their role in aging-associated metabolic changes by regulating NAD homeostasis.

Here, we report that M1 macrophages show increased CD38 expression, enhanced NADase activity, and production of NAD degradation byproducts NAM and ADPR. Using macrophages derived from WT and *Cd38* KO mice, we show that the high NADase activity of M1 macrophages is completely dependent on CD38 and not on other NAD consuming enzymes.

We report that CD38 expression is elevated in resident macrophages from epididymal white adipose tissue (eWAT) in old vs young mice. Lastly, we show that enhanced CD38 expression by tissue resident macrophages during aging is driven by the secretion of inflammatory factors by senescent cells. As senescent cells progressively accumulate in adipose tissue during aging, these results highlight a new causal link between visceral tissue senescence and tissue NAD decline during aging. Thus, suppressing CD38 expression and NADase activity by targeting macrophages and senescent cells may provide a therapeutic target to help restore NAD levels during aging.

Results:

Aging is associated with the accumulation of CD38 positive macrophages in adipose tissue

To verify that NAD levels decline in adipose tissue during aging, we measured NAD levels in epididymal white adipose tissue (eWAT) of mice at 6 months (young) and 25 months (old). We observed close to 50% reduction of NAD and NADP in old mice compared to young (Figure 1A), consistent with previous reports (Camacho-Pereira et al., 2016; Yoshino et al., 2011). Next, we analyzed CD38 expression in macrophages, the predominant immune cell in visceral adipose tissue (Xu et al., 2013), isolated from the stromal vascular fraction (SVF) of eWAT from old and young mice. As previously reported, flow cytometry analysis of the SVF can be used to distinguish resident and non-resident populations of adipose tissue macrophages (ATMs), based on cell surface markers expressed by macrophages, including F4/80 (EMR1) and CD11b (ITGAM) which are expressed by both resident and non-resident ATMs, and the integrin CD11c (ITGAX) which is expressed by non-resident ATMs (Cho et al., 2014; Xu et al., 2013). Using a similar gating strategy as Cho et al., and outlined in Figure 1B and S1A, we found a significant increase in the proportion of macrophages in the SVF of adipose tissue particularly after 12 months of age (Figure 1C). This increase was accounted for by an increase in the proportion of macrophages bearing a signature of resident macrophages (F4/80+, CD11b+, CD11c-), but not in the non-resident macrophage population (F4/80+, CD11b+, CD11c+) (Figure 1C). Interestingly, resident macrophages from older animals, but not the non-resident macrophages, showed progressively increased CD38 expression (Figure 1B, 1C, 1D and S1B). Although CD38 is also expressed by activated B and T cells, we did not see a significant increase in CD38 expression in non-macrophage immune cells in the SVF (CD45+, F4/80-, CD11b-) (Figure S1C). Taken together, these data show that age-related decline in eWAT NAD levels is correlated with enhanced expression of CD38 by resident adipose tissue macrophages (ATMs).

CD38 was recently identified as a marker of M1 macrophages (Jablonski et al., 2015). Thus, our data suggest that during aging, resident ATMs are polarizing from a M2 to M1-like phenotype. A similar switch from M2 to M1 macrophages has been reported during the metabolic stress of obesity (Lumeng et al., 2007). We therefore analyzed CD38 surface expression in macrophages from the eWAT of mice fed a high fat diet (HFD) or normal chow. In mice on a HFD diet, similar to aged mice, we saw an expected increase in total macrophages as a fraction of SVF (Figure S1D). In contrast to what we observed in aging, the fraction of resident macrophages present in SVF only increased modestly while the non-resident macrophages increased significantly (Figure S1D). Surprisingly, we observed the majority of resident ATMs from mice fed a high fat

diet had low levels of CD38 expression compared to mice fed a normal chow, while CD38+ non-resident macrophages were only a small fraction in both diets (Figure S1D). These results indicate that enhanced expression of CD38 by resident macrophages is unique to aged adipose tissue and that inflammation associated with obesity and aging are mediated via distinct mechanisms. These findings are consistent with a recent publication which showed CD38 is not enhanced in ATMs from obese mice or humans and that the inflammatory signaling pathways activated in M1-like macrophages during obesity are distinct from those induced by classical M1 polarization with pathogen-associated molecular patterns (PAMPs) such as lipopolysaccharide (LPS) (Kratz et al., 2014).

M1 macrophage polarization leads to increased expression of NAD hydrolases CD38 and CD157 and degradation of NAD

To test if different subsets of polarized macrophages have differential NADase activity, we polarized primary mouse bone marrow-derived macrophages (BMDMs) to the classical pro-inflammatory M1 macrophage with the bacterial endotoxin LPS and to the anti-inflammatory alternative activated M2 macrophage with the Th2 cytokine IL-4. Nicotinamide 1,N^6-etheno-adenine dinucleotide (ε-NAD) is a modified version of NAD in which cleavage of ε-NAD by an NAD hydrolase, such as CD38 or CD157, yields an increased fluorescence at 460nm that can be monitored over time. Incubating cellular lysates from untreated naïve (M0) or M2 macrophages showed no significant increase in fluorescence (Figure 2A). In contrast, M1 macrophage cellular lysates showed significantly increased fluorescence, consistent with increased NADase activity (Figure 2A and 2B).

Phenotypes in mouse and human macrophages can differ significantly (Murray et al., 2014). To test whether these observations applied to human macrophages, we measured NADase activity in M0, M1 and M2 macrophages derived from peripheral blood monocytes. We observed a similar increase in NAD hydrolysis in human M1 macrophages when compared to naïve and M2 subsets (Figure S2A). Taken together our data shows that enhanced NAD hydrolysis is a highly conserved feature of inflammatory M1 macrophages in both human and mice.

NAD is a critical regulator of metabolic pathways since it is the major hydride acceptor and co-factor for metabolic enzymes in glycolysis, TCA cycle, and glutaminolysis. Nutrient sensing and metabolic pathways are critical for macrophage activation, gene transcription, and other effector functions (Covarrubias et al., 2015; O'Neill and Pearce, 2016). The change in NAD hydrolase activity shown above suggested that different macrophage subtypes might exhibit different NAD levels. No reports have investigated how NAD levels might be linked to the metabolic reprogramming of macrophage metabolism or how NAD levels are affected in different macrophage polarization states. To address this question, we used targeted LC-MS to quantify the NAD metabolome in polarized macrophages. Importantly, other NAD-consuming enzymes such as PARPs, sirtuins, CD38 and CD157 all produce NAM as a byproduct of NAD hydrolysis. Consistent with the high NADase activity of M1 macrophages, we observed significantly elevated levels of NAM in M1 macrophages, but not in in naïve M0 and M2 macrophages (Figure 2C). Unexpectedly, elevated levels of NAD and NADP were observed in M2 macrophages but not in M1 macrophages (Figure 2C). This observation may be due to the

enhanced degradation of NAD by increased CD38 expression in M1 macrophages. Furthermore, NAD/NAM ratios were significantly lower in M1 macrophages (Figure 2D).

To identify the NAM-generating, NAD consuming enzyme(s) responsible for the high NADase activity in M1 macrophages, we measured mRNA expression of several key NAD consuming enzymes during a time course of macrophage differentiation. We observed that only *Cd38* (600-fold increase*)* and to a lesser degree its homologue *Cd157* (10-fold increase), but not *Sirt1, Parp1* and *Parp2* were significantly upregulated in M1 macrophages relative to naïve M0 and M2 macrophages (Figure 2E). A similar increase in *CD38* expression was also observed in human M1 macrophages (Figure S2B).

Despite the high NADase activity associated with M1 macrophages, their NAD levels seemed to be stably maintained compared to untreated naive macrophages (Figure 2C). This suggested that M1 macrophages might upregulate their biosynthetic and NAM salvage pathways to compensate for increased NAD degradation. The tissue culture medium used in our experiments lacks nicotinic acid but contains NAM. Under these conditions, NAD can be derived *de novo* from tryptophan or recycled from NAM via the NAM salvage pathway. Therefore, we measured mRNA levels of indoleamine 2,3-dioxygenase 1 (*Ido1)*, along with other key enzymes in the *de novo* NAD synthetic pathway (Figure 2E, S2C-D), and the NAM salvage pathway enzymes *Nampt* and nicotinamide mononucleotide adenylyltransferases 1-3 (*Nmnat1-3*) (Figure 2E). In M1 macrophages, we observed an increase in mRNA levels for *Nampt* and *Nmnat1*, which maintain nuclear NAD levels (Figure 2E). We did not see any significant changes in *Nmnat2* or *Nmnat3*, which regulate NAM salvage in the cytoplasm or mitochondria respectively, or in *Ido1* between M1 and M2 macrophages (Figure 2E). Interestingly, the gene expression of several key enzymes in the de novo synthesis pathway were downregulated during M1 polarization, including kynureninase (*Kynu*) and 3-hydroxy-anthranilic acid oxygenase (*Haao*) (Figure S2D). Furthermore, using LC-MS we observe increased levels of tryptophan, kynurenine and kynurenic acid in M1 macrophages compared to M0 and M2 macrophages (Figure S2E). However, we were unable to detect other tryptophan pathway metabolites downstream of kynurenine in either M0, M1 or M2 macrophages, which suggests, but does not prove, that tryptophan may not significantly contribute to *de novo* NAD synthesis in macrophages regardless of their differentiation stage (Figure S2E).

Such a possibility would predict a critical role for the NAD salvage pathway in maintenance of NAD levels in macrophages. Indeed, we observed that macrophages treated with FK866, a specific inhibitor of NAMPT (Figure 2F) showed a near complete suppression of NAD levels both in M1 and M2 macrophages (Figure 2G). Our data indicate that macrophages rely almost exclusively on the NAM salvage pathway to sustain their NAD levels and that M1 macrophages compensate for their enhanced NADase activity by increasing mRNA expression of key NAD salvage pathway enzymes, *Nampt* and *Nmnat1*.

NAM salvage pathway regulates NAD levels during M1 and M2 macrophage polarization to fine tune macrophage gene expression

In experiments described above, we consistently observed rising NAD levels during M2 polarization compared to M1 and M0 macrophages (Figure 2C). This result suggested that M2 polarization requires higher NAD levels. To test if NAD levels can regulate macrophage polarization, we pre-treated BMDMs with the NAMPT inhibitor FK866, to lower NAD levels (Figure 2G). This led to decreased mRNA expression of multiple canonical M2 markers (*Arg1*, *Mgl2*, *Ccl24* and *Fizz1*) (Figure 3A), however this was not universal since the M2 markers *Ym1* and *Cd36* were unaffected. In agreement with reduced expression of the gene *Arg1*, arginase activity, a key anti-inflammatory effector function of M2 macrophages, was also attenuated by FK866 (Figure 3B). We have previously shown that the same subset of FK866 sensitive M2 genes (*Arg1*, *Mgl2*, *Ccl24*, and *Fizz1*) are fine-tuned and integrated to metabolic inputs, while *Ym1* and *Cd36* are insensitive to metabolite levels including amino acids (Covarrubias et al., 2016). To confirm the role of NAD depletion, we supplemented macrophages treated with FK866 with different doses of nicotinamide mononucleotide (NMN) or nicotinamide riboside (NR) in the culture medium. Both NMN and NR are NAD precursors that feed into the NAM salvage pathway downstream of NAMPT (Figure 2F). Both rescued the mRNA expression of M2 genes inhibited by FK866 (Figure 3A and S3A) and arginase activity (Figure 3B) in a dose-dependent manner, with the exception of *Fizz1*. In contrast to a previous report (Van Gool et al., 2009), we observed that pre-treatment of macrophages with FK866 also suppressed mRNA expression and secretion of M1 inflammatory cytokines such as *Il-6* and *Tnf*α but not the metabolic enzyme *Irg1* (Figure 3C and 3D). NMN and NR also restored mRNA expression and protein levels of inflammatory cytokines in M1 macrophages (Figure 3C, 3D, and S3B). However, much higher concentrations of NMN (Figure 3A-D) and NR (Figure S3A and S3B) were needed to rescue FK866-sensitive M1 genes compared to M2 genes (Figure 3E). These results show that the NAM salvage pathway regulates NAD levels in macrophages, and that NAD is a critical regulator of macrophage polarization and regulates the mRNA abundance of a subset of M2 and M1 genes. Importantly, we show that M1 and M2 macrophages have different requirements for NAD levels, with M2 macrophages requiring higher levels of NAD to support M2 gene expression and effector functions (Figure 2E).

The NAD consuming enzyme CD38 is exclusively expressed by M1 macrophages and is the primary enzyme responsible for enhanced NAD hydrolase activity observed in M1 macrophages

To test the hypothesis that the high NADase activity observed in M1 macrophages is CD38-dependent, we first analyzed CD38 surface expression using flow cytometry in BMDMs. We compared M0, M1 and M2 macrophages obtained from wild type mice (WT) vs mice lacking CD38 (*Cd38* KO) (Cockayne et al., 1998). Consistent with the high *Cd38* mRNA levels and NADase activity associated with M1 macrophages (Figure 2), we found CD38 to be exclusively expressed by WT M1 macrophages (Figure 4A and S4A). Importantly, cell lysates from M1 macrophages lacking CD38 showed low NADase activity (Figures 4B and 4C). Importantly, PARP and sirtuin expression is unaffected in *Cd38* KO macrophages (Figure S4B). These data indicate that NADase activity of M1 macrophages specifically requires CD38, and not CD157 or any other NAD-consuming enzyme. CD38 can be localized to cell membranes in a type II and type III orientation, with its enzymatic domain facing outside (type II) or inside the cell (type III) (Liu et al., 2017; Shrimp et al., 2014; Zhao et al., 2012). To test whether the CD38 enzymatic

activity was predominantly localized to the extra- vs. intra-cellular space, we measured NAD degradation of the non-cell permeable εNAD in intact cells. We found that extracellular εNAD hydrolysis occurred only in M1 macrophages (Figure S4C), although to a lesser extent than what we observed in cell lysates (Figures 4C). These data demonstrate that CD38 cleaves NAD outside and inside cells and that a significant fraction of CD38 NADase activity in macrophages is intracellular.

To investigate how CD38 regulates intracellular NAD levels in macrophages, we quantified NAD and its metabolites in WT and *Cd38* KO BMDMs. We found that WT M1 macrophages had increased levels of NAM and ADP Ribose (ADPR), two specific products resulting from CD38 activity on NAD (Figure 4D). Importantly, the production of both metabolites was suppressed to basal levels in M1 macrophages derived from *Cd38* KOs (Figure 4D). *Cd38* KO M1 macrophages also had significantly higher levels of NAD and NADP and a higher NAD/NAM ratio compared to WT M1 macrophages (Figure 4D and 4E). Additionally, we found no significant differences in the levels of the nucleotides AMP and ADP in WT vs *Cd38* KO M1 macrophages (Figure 4D). Therefore, CD38 specifically consumes and regulates NAD metabolite levels and does affect the levels of other adenine-containing nucleotides. These data support the model that CD38 is a key regulator of NAD and its metabolites NAM and ADPR in M1 macrophages. These results seem to exclude a major role for CD157, whose mRNA is also increased in M1 macrophages (Figure 2E), as an NAD hydrolase. Interestingly, recent reports suggest the preferred CD157 substrate is the NAD precursor NR (Preugschat et al., 2014; Tarrago et al., 2018). In indirect support of this, we found that CD157 expression which was enhanced in response to LPS treatment was associated with significantly reduced NR levels in both WT and *Cd38* KO M1 macrophages (Figure S4D and S4E). Thus, although CD157 may indirectly influence NAD levels in M1 macrophages by consuming NR, the enhanced NADase activity of pro-inflammatory M1 macrophages is mediated by CD38.

Senescent cells promote macrophage CD38 expression and proliferation via the senescence associated secretory phenotype (SASP)

Cells enter senescence in response to diverse DNA damage and in response to oncogenic stimuli. Senescent cells are characterized by cell cycle arrest and by a complex senescence-associated secretory phenotype (SASP) that includes pro-inflammatory chemokines and cytokines (Coppe et al., 2010). Because senescent cells are produced in response to metabolic stress and accumulate during aging, they are thought to play a key role in the chronic inflammation and chronic diseases associated with aging (van Deursen, 2014). In support of this model, clearance of senescent cells extends lifespan and reverts age-related features in mice (Baker et al., 2016; Baker et al., 2011; Xu et al., 2018). Therefore, we sought to investigate whether cellular senescence influences macrophage polarization and CD38 expression during aging. In old mice (25 months), mRNA expression analysis of eWAT revealed increased expression of *Cd38*, senescence markers ($p16^{Ink4a}$, $p21^{Cip1}$), and SASP genes including inflammatory cytokines and chemokines (IL-6, IL-1β, IL-1α, IL-10 and Cxcl1) when compared to young mice (6 months) (Figure 5A and S5A). Consistent with the increased number of total macrophages detected in adipose tissue from aged mice (Figure 1C), we also observed an increase in the expression of the *Cd68* macrophage marker in old vs. young eWAT (Figure 5A).

Despite the increased numbers of macrophages in aged tissue, M2 macrophage markers trended down (such as *Arg1*, *Fizz1* and *Mgl2*) or were unchanged (*Ccl24*) (Figure 5A). Thus, compared to young mice, we found adipose tissue from old animals to be significantly more inflamed, have increased accumulation of senescent cells, and a shift in macrophage polarization from M2 to a M1-like state.

Senescence can also be induced by intraperitoneal injection (IP) of young mice with the chemotherapeutic agent doxorubicin. Doxorubicin intercalates into DNA and inhibits topoisomerase II activity, inducing cellular senescence both in tissue culture and *in vivo* (Demaria et al., 2017; Pommier et al., 2010). In doxorubicin treated mice, mRNA expression of *Cd38* in eWAT was increased in parallel with senescence markers (p16 and p21) and inflammatory cytokines and chemokines (Figure 5B and S5B), similar to that observed during aging (Figure 5A). Flow cytometry of macrophages extracted from eWAT from doxorubicin-treated mice showed increased macrophage accumulation compared to control mice (Figure 5C and S5C). Furthermore, doxorubicin treatment also led to increased CD38+ resident and non-resident macrophages (Figure 5C). These results support the model that senescent cells and associated chronic inflammation is a key mechanism for increased CD38 expression in ATMs from eWAT.

To test the hypothesis that SASP from senescent cells drives CD38 expression in macrophages, we induced senescence in mouse dermal fibroblasts (MDFs) by irradiation (IRR-MDF) or doxorubicin (Doxo-MDF) and purified conditioned media (Baar et al., 2017; Demaria et al., 2017). Macrophages cultured for 24 hours in conditioned media from senescent cells specifically upregulate *Cd38* and to a lesser extent *Cd157*, but not other NAD consuming enzymes including *Parp1*, *Parp2*, *Sirt1* and *Sirt2* (Figure 5D). Consistent with this observation, co-culturing WT macrophages with senescent cells derived from irradiated mouse dermal fibroblasts increased *Cd38* expression to a similar extent (Figure S5D). This did not occur in WT macrophages co-cultured with non-senescent MDFs or in *Cd38* KO macrophages (Figure S5D). Furthermore, we did not observe a significant increase in *Cd38* mRNA levels in senescent cells alone compared to non-senescent MDFs (Figure S5D).

Increased CD38 expression and enhanced NADase activity occurs in response to LPS-driven activation of toll-like receptor 4 (TLR4) in macrophages (Figure 2 and 4) and during a programmed immune response to pathogens (Matalonga et al., 2017). In addition to senescent cell accumulation and their SASP, pathogen associated molecular patterns (PAMPs) may represent another source of inflammation during aging. A recent study showed that gut intestinal barrier permeability is increased during aging and which can lead to significantly higher levels of endotoxins, including LPS, in aging tissues (Buford, 2017; Thevaranjan et al., 2017). To test whether other TLR ligands besides LPS can increase *Cd38* mRNA expression in macrophages, we treated BMDMs with multiple TLR ligands including Pam3CSK4 (P3C4) (TLR1/2), heat-killed Listeria monocytogenes (HKLM)(TLR2), poly(I:C)-high and low molecular weight (TLR3), LPS (TLR4), flagellin *S. typhimurium* (FLA-ST) (TLR5), synthetic lipopeptide FSL-1 (TLR 6/2), ssRNA (TLR7) and CpG oligonucleotide ODN1826 (TLR9). With the exception of poly(I:C), a synthetic double stranded RNA that mimics viral RNA, all TLR ligands highly activated *Cd38*

mRNA expression (Figure 5E). In addition to PAMPs, endogenous alarmin molecules derived from damaged or dead cells, known as danger associated molecular patterns (DAMPs), are an important source of sterile inflammation and have been reported to activate TLRs (Schaefer, 2014). Senescent human and mouse fibroblasts secrete nuclear protein HMGB1, a DAMP which can activate TLR4 in addition to RAGE (Receptor for advanced glycation end products) to promote inflammatory signaling pathways (Davalos et al., 2013). Surprisingly, treatment of BMDMs with multiple DAMPs including HMGB1did not activate CD38 expression (Figure 5F), suggesting that individual DAMPs may not be a mechanism of CD38 activation in macrophages.

In addition to DAMPs, cytokines such as type 1 interferons (IFNα/IFNβ) have also been reported to drive CD38 expression in mouse and human macrophages (Kratz et al., 2014).
We observed that IRR-MDF senescent cells significantly up-regulate transcription of *Ifnα*, along with other inflammatory cytokines (*Tnfα, Il-12, Il-6,* and *Il-10*) (Figure 5G) compared to normal MDF cells. Therefore, we treated BMDMs with these recombinant cytokines and measured CD38 (Figure 5H). Interestingly, TNF-α, IL-6, and IL-10 were able to promote CD38 expression, while IFNα, IFNβ, and IL-12 did not (Figure 5H). The inability of type-1 interferons to promote CD38 expression are consistent with our poly(I:C) data (Figure 5E). The poly(I:C) receptor TLR3 is the only TLR whose signaling is MYD88-independent and signals through IRF3, which leads to upregulation of type 1 interferons and interferon inducible genes (Chin et al., 2010), but not CD38 (Figure 5H). These observations support the model that the combined activities of TLR activation by pathogen ligands and sterile sources of inflammation such as SASP enhance CD38 expression and may contribute to decreased tissue NAD levels.

Lastly, we showed that aging leads to the accumulation of resident macrophages in mouse eWAT (Figure 1C). Resident macrophages, such as ATMs, are seeded in tissues during development and have the capacity to self-renew, which is driven by CSF1 and other growth factors including MCP-1 and IL-4 during helminth infections (Amano et al., 2014; Davies et al., 2013; Ginhoux et al., 2010; Hashimoto et al., 2013; Jenkins et al., 2011). Interestingly, senescent fibroblasts highly express CSF1 (Figure 5G) and other growth factors (Coppe et al., 2010). Therefore, to test if SASP can promote macrophage proliferation, we treated BMDMs with SASP derived from IRR-MDFs or control media and measured cell proliferation with the fluorescent thymidine analogue EdU which is incorporated into DNA during active synthesis (Figure 5I). We observed a 3-fold increase in Edu+ macrophages upon treatment with SASP compared to conditioned media from non-senescent MDFs (Figure 5I). This enhanced proliferation resulted in higher cell confluency after just 24 hours of SASP exposure (Figure 5J). Taken together, our data show that SASP is sufficient to drive expression of the NAD hydrolase CD38 in macrophages as well as increase the total macrophage population by promoting macrophage proliferation.

Discussion:
There is growing evidence that NAD levels decline during aging. However, the mechanism and connections to episodes of metabolic stress are poorly understood. CD38 has recently emerged as a key NAD consuming enzyme that is upregulated during aging. Loss of CD38 activity in *Cd38 KO* mice or in mice treated with a CD38-specific inhibitor, 78c, are protected from age-

related NAD decline and show improved metabolic health (Camacho-Pereira et al., 2016; Tarrago et al., 2018). Therefore, blocking CD38 NADase activity is emerging as a promising therapeutic target to suppress NAD loss associated with aging (Chini et al., 2018). In this study, we investigated which cell types show increased expression of CD38 during aging and the mechanism(s) responsible for this enhanced CD38 expression.

We determined that aging-related inflammation drives the polarization of tissue resident macrophages to an M1-like state characterized by the increased expression of CD38 and enhanced consumption of NAD (Figure 6). As organisms age, DNA damage and genotoxic stress accumulates, leading some cells to undergo cell cycle arrest and senescence. Although senescent cells can play beneficial roles in wound healing and embryogenesis, they also secrete inflammatory factors or SASP that disrupt normal cellular functions, damage tissues, and may promote carcinogenesis (Campisi, 2013; Campisi and Robert, 2014). Here, we provide evidence that SASP is also sufficient to increase CD38 expression in macrophages and promote macrophage proliferation, leading to increased accumulation of CD38+ macrophages in both naturally aged mice and in young mice with increased senescent cell burden following treatment with the chemotherapeutic agent doxorubicin (Figure 5). These results provide a key link between the accumulation of senescent cells in aged tissues and age-related NAD decline. Interestingly, recent studies using senolytics or genetically engineered mouse models, such as p16-3MR and INK-ATTAC mice, have shown that selective killing of senescent cells during aging leads to delayed aging-related diseases and increased healthspan (Baker et al., 2016; Baker et al., 2011; Demaria et al., 2014; Xu et al., 2018). Our data suggest that some of the health benefits derived from eliminating senescent cells may occur as a result of reduced CD38 expression in tissue resident macrophages leading to NAD repletion. Our study also raises new questions on how senescent cells and macrophages communicate and how their interactions influence each other's function. While we showed that SASP, in particular immunomodulatory cytokines such as IL-6, TNFα, and IL-10, can promote CD38 expression in macrophages (Figure 5G-H), it will be important to more thoroughly investigate other components of the SASP to identify additional factors which activate CD38 expression in macrophages. In addition to sterile sources of inflammation such as SASP, we showed that a variety of PAMPs can also promote CD38 expression (Figure 5E). Since aging is associated with a loss of gut epithelial barrier integrity, or "leaky gut" (Thevaranjan et al., 2017), endotoxins from commensal bacteria may also synergize with SASP to promote inflammation during aging and/or infection and enhance expression of CD38. Therefore, future studies will be necessary to better understand and dissociate sterile and non-sterile drivers of inflammation and how each influences CD38 expression and NAD hydrolysis.

In older mice with lower tissue NAD levels and hyper CD38 expression/NAD hydrolase activity, Sirt3 activity is reduced leading to increased mitochondrial dysfunction (Camacho-Pereira et al., 2016). Sirt3-dependent mitochondrial dysfunction promotes cellular senescence and regulates the secretion of a subset of SASP (Wiley et al., 2016). Furthermore, it was recently reported that NAD repletion in older mice leads to NAD binding to the NHD domain of DBC1, releasing its suppression of PARP1 and thereby allowing PARP1 to facilitate DNA repair (Li et al., 2017). During aging and episodes of metabolic stress, enhanced CD38 NADase activity by

macrophages and depletion of local tissue NAD levels may promote the accumulation of senescent cells as a result of reduced activity of sirtuins and other NAD consuming enzymes such as PARP1. More senescent cells would mean greater SASP in local tissues, creating a positive feedback cycle which further drives the expression of CD38 and inflammatory cytokines, thus resulting in enhanced inflammation, depletion of NAD, and increased cellular senescence. Future studies will determine if drugs targeting CD38, such as 78c, can break this cycle and lead to reduced cellular senescence in aged mice.

Another question our study raises is what role CD38 plays in modulating immune cell function. There have been limited studies showing that CD38 regulates immune cell homing, innate immune responses to pathogens, and anti-tumor immunity (Chatterjee et al., 2018; Lischke et al., 2013; Partida-Sanchez et al., 2007). However, *Cd38* remains a largely uncharacterized gene in immunology, despite its widespread use in the field as an activation marker. While the teleological purpose of increased NAD consumption by CD38+ M1 macrophages is not obvious, it is tempting to speculate that degradation of NAD may influence NAD levels for control of other NAD consuming enzymes such as PARPs and sirtuins (discussed above) or downstream processes that are dependent on secondary messaging properties of CD38-derived NAD metabolites, such as cADPR for control of Ca2+ mobilization (Wei et al., 2014). In addition, NAM exhibits immunomodulatory properties and high levels of NAM can reduce inflammatory cytokine production in macrophages (Weiss et al., 2015), suggesting that CD38 may act as a feedback mechanism to initiate the resolution of acute inflammation. This negative feedback mechanism may become maladaptive during aging.

Using a specific inhibitor of NAMPT, a key enzyme in NAD salvage, we also show that NAD levels regulate macrophage polarization and that M1 and M2 macrophages appear to have different requirements in terms of NAD (Figure 5 and 6). M2 macrophage polarization requires higher levels of NAD precursors to support the gene transcription of a subset of M2 genes than M1 macrophages (greater than 0.5mM NMN/NR for M2 genes vs 100μM for M1 genes) (Figure 3E). Our results, showing that NAD levels can regulate macrophage gene transcription are at odds with a previous report showing that inhibiting NAMPT did not affect gene transcription. This disparity may reflect the difference in the mouse macrophage-like cell lines (Raw 264.7) used in their study vs the primary BMDMs used in our study (Van Gool et al., 2009). Our findings bring up additional questions of how NAD levels may influence macrophage activation and gene transcription. Interestingly, sirtuins have also been shown to regulate macrophage polarization (Lo Sasso et al., 2014; Yoshizaki et al., 2010), and their activity is directly linked to NAD levels. Future studies should investigate whether increased NAD levels in M2 macrophages are necessary to promote sirtuin activity. Lastly, NR and NMN supplements have been shown to increase NAD levels and to increase health span and life span in mice (Yoshino et al., 2018), and are becoming popular supplements to promote healthy aging in humans. Therefore, it will be necessary to understand how restoring NAD levels with these supplements, and potentially with CD38 inhibitors such as 78c, affects macrophage polarization and immune system function.

In conclusion, our study demonstrates that increased expression of CD38 in macrophages represents an important source of increased NADase activity during aging. These data also provide insight into how the immune system and NAD metabolism are integrated. While our study focused on visceral white adipose tissue, we speculate that a similar mechanism linking SASP to macrophage CD38 NADase activity is responsible for NAD declines in other tissues, particularly those where macrophages reside in high abundance such as the liver and brain. This newly discovered cross-talk between senescent cells and macrophages which modulates tissue NAD levels may provide a therapeutic avenue to target age-related inflammation and help restore NAD levels and metabolic health in aging individuals.

Author Contributions:
Conceptualization A.J.C. and E.V.; Methodology, A.J.C. and E.V.; Investigation, A.J.C. (all experiments), J.A.L.D. (In vivo experiments), A.K. (senescent cell experiments), R.P. (NADase Assays and Flow Cytometry), J.N. (In Vivo experiments), S.I. (RNA analysis), M.S. (LC-MS), H.K. (Flow Cytometry), I.B.S. (LC-MS), M.O. (Animal Housing), C.B. (LC-MS), J.C. (Senescent cell experiments); Writing – Original Draft, A.J.C. and E.V.; Writing – Review & Editing, all authors; Supervision, E.V.; Funding Acquisition, E.V.

Declaration of Interest: All authors have reviewed and approved the manuscript. C.B. is the inventor of intellectual property on the nutritional and therapeutic uses of NR, serves as chief scientific advisor of and holds stock in ChromaDex.

Acknowledgements:
This project was supported by the NIH grant R24DK085610 (E.V.), Gladstone Institute intramural funds (E.V.), and Buck Institute intramural funds (E.V.). A.J.C. is a recipient of the UC President's Postdoctoral Fellowship at UCSF and is also supported by a NIH T32 training grant (3T32AG000266-19S1). We thank Marius Walter for his help imaging cells. We thank Mark Watson from the Martin Brand Lab for providing us with adipose tissue from mice on a high fat diet and control fed mice. We thank Vanessa Byles and Davalyn Powell for reviewing the manuscript and helpful discussion.

References:
Amano, S.U., Cohen, J.L., Vangala, P., Tencerova, M., Nicoloro, S.M., Yawe, J.C., Shen, Y., Czech, M.P., and Aouadi, M. (2014). Local proliferation of macrophages contributes to obesity-associated adipose tissue inflammation. Cell Metab *19*, 162-171.
Baar, M.P., Brandt, R.M.C., Putavet, D.A., Klein, J.D.D., Derks, K.W.J., Bourgeois, B.R.M., Stryeck, S., Rijksen, Y., van Willigenburg, H., Feijtel, D.A.*, et al.* (2017). Targeted Apoptosis of Senescent Cells Restores Tissue Homeostasis in Response to Chemotoxicity and Aging. Cell *169*, 132-147 e116.
Baker, D.J., Childs, B.G., Durik, M., Wijers, M.E., Sieben, C.J., Zhong, J., Saltness, R.A., Jeganathan, K.B., Verzosa, G.C., Pezeshki, A.*, et al.* (2016). Naturally occurring p16(Ink4a)-positive cells shorten healthy lifespan. Nature *530*, 184-189.
Baker, D.J., Wijshake, T., Tchkonia, T., LeBrasseur, N.K., Childs, B.G., van de Sluis, B., Kirkland, J.L., and van Deursen, J.M. (2011). Clearance of p16Ink4a-positive senescent cells delays ageing-associated disorders. Nature *479*, 232-236.

Belenky, P., Bogan, K.L., and Brenner, C. (2007). NAD+ metabolism in health and disease. Trends Biochem Sci *32*, 12-19.
Bogan, K.L., and Brenner, C. (2008). Nicotinic Acid, Nicotinamide and Nicotinamide Riboside: A Molecular Evaluation of NAD+ Precursor Vitamins in Human Nutrition. Ann Review Nutrition *28*, 115-130.
Buford, T.W. (2017). (Dis)Trust your gut: the gut microbiome in age-related inflammation, health, and disease. Microbiome *5*, 80.
Byles, V., Covarrubias, A.J., Ben-Sahra, I., Lamming, D.W., Sabatini, D.M., Manning, B.D., and Horng, T. (2013). The TSC-mTOR pathway regulates macrophage polarization. Nat Commun *4*, 2834.
Camacho-Pereira, J., Tarrago, M.G., Chini, C.C.S., Nin, V., Escande, C., Warner, G.M., Puranik, A.S., Schoon, R.A., Reid, J.M., Galina, A.*, et al.* (2016). CD38 Dictates Age-Related NAD Decline and Mitochondrial Dysfunction through an SIRT3-Dependent Mechanism. Cell Metab *23*, 1127-1139.
Campisi, J. (2013). Aging, cellular senescence, and cancer. Annu Rev Physiol *75*, 685-705.
Campisi, J., and Robert, L. (2014). Cell senescence: role in aging and age-related diseases. Interdiscip Top Gerontol *39*, 45-61.
Canto, C., Menzies, K.J., and Auwerx, J. (2015). NAD(+) Metabolism and the Control of Energy Homeostasis: A Balancing Act between Mitochondria and the Nucleus. Cell Metab *22*, 31-53.
Chatterjee, S., Daenthanasanmak, A., Chakraborty, P., Wyatt, M.W., Dhar, P., Selvam, S.P., Fu, J., Zhang, J., Nguyen, H., Kang, I.*, et al.* (2018). CD38-NAD(+)Axis Regulates Immunotherapeutic Anti-Tumor T Cell Response. Cell Metab *27*, 85-100 e108.
Chin, A.I., Miyahira, A.K., Covarrubias, A., Teague, J., Guo, B., Dempsey, P.W., and Cheng, G. (2010). Toll-like receptor 3-mediated suppression of TRAMP prostate cancer shows the critical role of type I interferons in tumor immune surveillance. Cancer Res *70*, 2595-2603.
Chini, E.N., Chini, C.C.S., Espindola Netto, J.M., de Oliveira, G.C., and van Schooten, W. (2018). The Pharmacology of CD38/NADase: An Emerging Target in Cancer and Diseases of Aging. Trends Pharmacol Sci *39*, 424-436.
Cho, K.W., Morris, D.L., and Lumeng, C.N. (2014). Flow cytometry analyses of adipose tissue macrophages. Methods Enzymol *537*, 297-314.
Cockayne, D.A., Muchamuel, T., Grimaldi, J.C., Muller-Steffner, H., Randall, T.D., Lund, F.E., Murray, R., Schuber, F., and Howard, M.C. (1998). Mice deficient for the ecto-nicotinamide adenine dinucleotide glycohydrolase CD38 exhibit altered humoral immune responses. Blood *92*, 1324-1333.
Coppe, J.P., Desprez, P.Y., Krtolica, A., and Campisi, J. (2010). The senescence-associated secretory phenotype: the dark side of tumor suppression. Annu Rev Pathol *5*, 99-118.
Covarrubias, A.J., Aksoylar, H.I., and Horng, T. (2015). Control of macrophage metabolism and activation by mTOR and Akt signaling. Semin Immunol *27*, 286-296.
Covarrubias, A.J., Aksoylar, H.I., Yu, J., Snyder, N.W., Worth, A.J., Iyer, S.S., Wang, J., Ben-Sahra, I., Byles, V., Polynne-Stapornkul, T.*, et al.* (2016). Akt-mTORC1 signaling regulates Acly to integrate metabolic input to control of macrophage activation. Elife *5*.
Davalos, A.R., Kawahara, M., Malhotra, G.K., Schaum, N., Huang, J., Ved, U., Beausejour, C.M., Coppe, J.P., Rodier, F., and Campisi, J. (2013). p53-dependent release of Alarmin HMGB1 is a central mediator of senescent phenotypes. J Cell Biol *201*, 613-629.
Davies, L.C., Rosas, M., Jenkins, S.J., Liao, C.T., Scurr, M.J., Brombacher, F., Fraser, D.J., Allen, J.E., Jones, S.A., and Taylor, P.R. (2013). Distinct bone marrow-derived and tissue-resident macrophage lineages proliferate at key stages during inflammation. Nat Commun *4*, 1886.
Demaria, M., O'Leary, M.N., Chang, J., Shao, L., Liu, S., Alimirah, F., Koenig, K., Le, C., Mitin, N., Deal, A.M.*, et al.* (2017). Cellular Senescence Promotes Adverse Effects of Chemotherapy and Cancer Relapse. Cancer Discov *7*, 165-176.

Demaria, M., Ohtani, N., Youssef, S.A., Rodier, F., Toussaint, W., Mitchell, J.R., Laberge, R.M., Vijg, J., Van Steeg, H., Dolle, M.E., *et al.* (2014). An essential role for senescent cells in optimal wound healing through secretion of PDGF-AA. Dev Cell *31*, 722-733.
Franceschi, C., Bonafe, M., Valensin, S., Olivieri, F., De Luca, M., Ottaviani, E., and De Benedictis, G. (2000). Inflamm-aging. An evolutionary perspective on immunosenescence. Ann N Y Acad Sci *908*, 244-254.
Franceschi, C., and Campisi, J. (2014). Chronic inflammation (inflammaging) and its potential contribution to age-associated diseases. J Gerontol A Biol Sci Med Sci *69 Suppl 1*, S4-9.
Ganeshan, K., and Chawla, A. (2014). Metabolic regulation of immune responses. Annu Rev Immunol *32*, 609-634.
Ginhoux, F., Greter, M., Leboeuf, M., Nandi, S., See, P., Gokhan, S., Mehler, M.F., Conway, S.J., Ng, L.G., Stanley, E.R., *et al.* (2010). Fate mapping analysis reveals that adult microglia derive from primitive macrophages. Science *330*, 841-845.
Harden, A.Y., W.J. (1906). The alcoholic ferment of yeast-juice. Proceedings of the Royal Society B: Biological Sciences.
Hashimoto, D., Chow, A., Noizat, C., Teo, P., Beasley, M.B., Leboeuf, M., Becker, C.D., See, P., Price, J., Lucas, D., *et al.* (2013). Tissue-resident macrophages self-maintain locally throughout adult life with minimal contribution from circulating monocytes. Immunity *38*, 792-804.
Hotamisligil, G.S. (2017). Inflammation, metaflammation and immunometabolic disorders. Nature *542*, 177-185.
Huang, Y., Louie, A., Yang, Q., Massenkoff, N., Xu, C., Hunt, P.W., and Gee, W. (2013). A simple LC-MS/MS method for determination of kynurenine and tryptophan concentrations in human plasma from HIV-infected patients. Bioanalysis *5*, 1397-1407.
Jablonski, K.A., Amici, S.A., Webb, L.M., Ruiz-Rosado Jde, D., Popovich, P.G., Partida-Sanchez, S., and Guerau-de-Arellano, M. (2015). Novel Markers to Delineate Murine M1 and M2 Macrophages. PLoS One *10*, e0145342.
Jackson, D.G., and Bell, J.I. (1990). Isolation of a cDNA encoding the human CD38 (T10) molecule, a cell surface glycoprotein with an unusual discontinuous pattern of expression during lymphocyte differentiation. J Immunol *144*, 2811-2815.
Jenkins, S.J., Ruckerl, D., Cook, P.C., Jones, L.H., Finkelman, F.D., van Rooijen, N., MacDonald, A.S., and Allen, J.E. (2011). Local macrophage proliferation, rather than recruitment from the blood, is a signature of TH2 inflammation. Science *332*, 1284-1288.
Kim, M.Y., Zhang, T., and Kraus, W.L. (2005). Poly(ADP-ribosyl)ation by PARP-1: 'PAR-laying' NAD+ into a nuclear signal. Genes Dev *19*, 1951-1967.
Kratz, M., Coats, B.R., Hisert, K.B., Hagman, D., Mutskov, V., Peris, E., Schoenfelt, K.Q., Kuzma, J.N., Larson, I., Billing, P.S., *et al.* (2014). Metabolic dysfunction drives a mechanistically distinct proinflammatory phenotype in adipose tissue macrophages. Cell Metab *20*, 614-625.
Lewis, C.A., Parker, S.J., Fiske, B.P., McCloskey, D., Gui, D.Y., Green, C.R., Vokes, N.I., Feist, A.M., Vander Heiden, M.G., and Metallo, C.M. (2014). Tracing compartmentalized NADPH metabolism in the cytosol and mitochondria of mammalian cells. Mol Cell *55*, 253-263.
Li, B., Navarro, S., Kasahara, N., and Comai, L. (2004). Identification and biochemical characterization of a Werner's syndrome protein complex with Ku70/80 and poly(ADP-ribose) polymerase-1. J Biol Chem *279*, 13659-13667.
Li, J., Bonkowski, M.S., Moniot, S., Zhang, D., Hubbard, B.P., Ling, A.J., Rajman, L.A., Qin, B., Lou, Z., Gorbunova, V., *et al.* (2017). A conserved NAD(+) binding pocket that regulates protein-protein interactions during aging. Science *355*, 1312-1317.
Lischke, T., Heesch, K., Schumacher, V., Schneider, M., Haag, F., Koch-Nolte, F., and Mittrucker, H.W. (2013). CD38 controls the innate immune response against Listeria monocytogenes. Infect Immun *81*, 4091-4099.

Liu, J., Zhao, Y.J., Li, W.H., Hou, Y.N., Li, T., Zhao, Z.Y., Fang, C., Li, S.L., and Lee, H.C. (2017). Cytosolic interaction of type III human CD38 with CIB1 modulates cellular cyclic ADP-ribose levels. Proc Natl Acad Sci U S A.

Liu, L., Su, X., Quinn, W.J., 3rd, Hui, S., Krukenberg, K., Frederick, D.W., Redpath, P., Zhan, L., Chellappa, K., White, E.*, et al.* (2018). Quantitative Analysis of NAD Synthesis-Breakdown Fluxes. Cell Metab *27*, 1067-1080 e1065.

Lo Sasso, G., Menzies, K.J., Mottis, A., Piersigilli, A., Perino, A., Yamamoto, H., Schoonjans, K., and Auwerx, J. (2014). SIRT2 deficiency modulates macrophage polarization and susceptibility to experimental colitis. PLoS One *9*, e103573.

Lopez-Otin, C., Blasco, M.A., Partridge, L., Serrano, M., and Kroemer, G. (2013). The hallmarks of aging. Cell *153*, 1194-1217.

Lumeng, C.N., Bodzin, J.L., and Saltiel, A.R. (2007). Obesity induces a phenotypic switch in adipose tissue macrophage polarization. J Clin Invest *117*, 175-184.

Matalonga, J., Glaria, E., Bresque, M., Escande, C., Carbo, J.M., Kiefer, K., Vicente, R., Leon, T.E., Beceiro, S., Pascual-Garcia, M.*, et al.* (2017). The Nuclear Receptor LXR Limits Bacterial Infection of Host Macrophages through a Mechanism that Impacts Cellular NAD Metabolism. Cell Rep *18*, 1241-1255.

Mitchell, S.J., Bernier, M., Aon, M.A., Cortassa, S., Kim, E.Y., Fang, E.F., Palacios, H.H., Ali, A., Navas-Enamorado, I., Di Francesco, A.*, et al.* (2018). Nicotinamide Improves Aspects of Healthspan, but Not Lifespan, in Mice. Cell Metab *27*, 667-676 e664.

Mouchiroud, L., Houtkooper, R.H., Moullan, N., Katsyuba, E., Ryu, D., Canto, C., Mottis, A., Jo, Y.S., Viswanathan, M., Schoonjans, K.*, et al.* (2013). The NAD(+)/Sirtuin Pathway Modulates Longevity through Activation of Mitochondrial UPR and FOXO Signaling. Cell *154*, 430-441.

Murano, I., Barbatelli, G., Parisani, V., Latini, C., Muzzonigro, G., Castellucci, M., and Cinti, S. (2008). Dead adipocytes, detected as crown-like structures, are prevalent in visceral fat depots of genetically obese mice. J Lipid Res *49*, 1562-1568.

Murray, P.J., Allen, J.E., Biswas, S.K., Fisher, E.A., Gilroy, D.W., Goerdt, S., Gordon, S., Hamilton, J.A., Ivashkiv, L.B., Lawrence, T.*, et al.* (2014). Macrophage activation and polarization: nomenclature and experimental guidelines. Immunity *41*, 14-20.

O'Neill, L.A., and Pearce, E.J. (2016). Immunometabolism governs dendritic cell and macrophage function. J Exp Med *213*, 15-23.

Partida-Sanchez, S., Gasser, A., Fliegert, R., Siebrands, C.C., Dammermann, W., Shi, G., Mousseau, B.J., Sumoza-Toledo, A., Bhagat, H., Walseth, T.F.*, et al.* (2007). Chemotaxis of mouse bone marrow neutrophils and dendritic cells is controlled by adp-ribose, the major product generated by the CD38 enzyme reaction. J Immunol *179*, 7827-7839.

Pommier, Y., Leo, E., Zhang, H., and Marchand, C. (2010). DNA topoisomerases and their poisoning by anticancer and antibacterial drugs. Chem Biol *17*, 421-433.

Preugschat, F., Carter, L.H., Boros, E.E., Porter, D.J., Stewart, E.L., and Shewchuk, L.M. (2014). A pre-steady state and steady state kinetic analysis of the N-ribosyl hydrolase activity of hCD157. Arch Biochem Biophys *564*, 156-163.

Quarona, V., Zaccarello, G., Chillemi, A., Brunetti, E., Singh, V.K., Ferrero, E., Funaro, A., Horenstein, A.L., and Malavasi, F. (2013). CD38 and CD157: a long journey from activation markers to multifunctional molecules. Cytometry B Clin Cytom *84*, 207-217.

Reinherz, E.L., Kung, P.C., Goldstein, G., Levey, R.H., and Schlossman, S.F. (1980). Discrete stages of human intrathymic differentiation: analysis of normal thymocytes and leukemic lymphoblasts of T-cell lineage. Proc Natl Acad Sci U S A *77*, 1588-1592.

Savarino, A., Bottarel, F., Malavasi, F., and Dianzani, U. (2000). Role of CD38 in HIV-1 infection: an epiphenomenon of T-cell activation or an active player in virus/host interactions? AIDS *14*, 1079-1089.

Schaefer, L. (2014). Complexity of danger: the diverse nature of damage-associated molecular patterns. J Biol Chem *289*, 35237-35245.

Scheibye-Knudsen, M., Mitchell, S.J., Fang, E.F., Iyama, T., Ward, T., Wang, J., Dunn, C.A., Singh, N., Veith, S., Hasan-Olive, M.M., *et al.* (2014). A high-fat diet and NAD(+) activate Sirt1 to rescue premature aging in cockayne syndrome. Cell Metab *20*, 840-855.
Schneider, M., Schumacher, V., Lischke, T., Lucke, K., Meyer-Schwesinger, C., Velden, J., Koch-Nolte, F., and Mittrucker, H.W. (2015). CD38 is expressed on inflammatory cells of the intestine and promotes intestinal inflammation. PLoS One *10*, e0126007.
Shrimp, J.H., Hu, J., Dong, M., Wang, B.S., MacDonald, R., Jiang, H., Hao, Q., Yen, A., and Lin, H. (2014). Revealing CD38 cellular localization using a cell permeable, mechanism-based fluorescent small-molecule probe. J Am Chem Soc *136*, 5656-5663.
Sica, A., and Mantovani, A. (2012). Macrophage plasticity and polarization: in vivo veritas. J Clin Invest *122*, 787-795.
Tarrago, M.G., Chini, C.C.S., Kanamori, K.S., Warner, G.M., Caride, A., de Oliveira, G.C., Rud, M., Samani, A., Hein, K.Z., Huang, R., *et al.* (2018). A Potent and Specific CD38 Inhibitor Ameliorates Age-Related Metabolic Dysfunction by Reversing Tissue NAD(+) Decline. Cell Metab *27*, 1081-1095 e1010.
Thevaranjan, N., Puchta, A., Schulz, C., Naidoo, A., Szamosi, J.C., Verschoor, C.P., Loukov, D., Schenck, L.P., Jury, J., Foley, K.P., *et al.* (2017). Age-Associated Microbial Dysbiosis Promotes Intestinal Permeability, Systemic Inflammation, and Macrophage Dysfunction. Cell Host Microbe *21*, 455-466 e454.
Trammell, S.A., and Brenner, C. (2013). Targeted, LCMS-based Metabolomics for Quantitative Measurement of NAD(+) Metabolites. Comput Struct Biotechnol J *4*, e201301012.
Trammell, S.A., Schmidt, M.S., Weidemann, B.J., Redpath, P., Jaksch, F., Dellinger, R.W., Li, Z., Abel, E.D., Migaud, M.E., and Brenner, C. (2016). Nicotinamide riboside is uniquely and orally bioavailable in mice and humans. Nat Commun *7*, 12948.
van Deursen, J.M. (2014). The role of senescent cells in ageing. Nature *509*, 439-446.
Van Gool, F., Galli, M., Gueydan, C., Kruys, V., Prevot, P.P., Bedalov, A., Mostoslavsky, R., Alt, F.W., De Smedt, T., and Leo, O. (2009). Intracellular NAD levels regulate tumor necrosis factor protein synthesis in a sirtuin-dependent manner. Nat Med *15*, 206-210.
Verdin, E. (2015). NAD(+) in aging, metabolism, and neurodegeneration. Science *350*, 1208-1213.
Wei, W., Graeff, R., and Yue, J. (2014). Roles and mechanisms of the CD38/cyclic adenosine diphosphate ribose/Ca(2+) signaling pathway. World J Biol Chem *5*, 58-67.
Weisberg, S.P., McCann, D., Desai, M., Rosenbaum, M., Leibel, R.L., and Ferrante, A.W., Jr. (2003). Obesity is associated with macrophage accumulation in adipose tissue. J Clin Invest *112*, 1796-1808.
Weiss, R., Schilling, E., Grahnert, A., Kolling, V., Dorow, J., Ceglarek, U., Sack, U., and Hauschildt, S. (2015). Nicotinamide: a vitamin able to shift macrophage differentiation toward macrophages with restricted inflammatory features. Innate Immun *21*, 813-826.
Wiley, C.D., Velarde, M.C., Lecot, P., Liu, S., Sarnoski, E.A., Freund, A., Shirakawa, K., Lim, H.W., Davis, S.S., Ramanathan, A., *et al.* (2016). Mitochondrial Dysfunction Induces Senescence with a Distinct Secretory Phenotype. Cell Metab *23*, 303-314.
Xu, H., Barnes, G.T., Yang, Q., Tan, G., Yang, D., Chou, C.J., Sole, J., Nichols, A., Ross, J.S., Tartaglia, L.A., *et al.* (2003). Chronic inflammation in fat plays a crucial role in the development of obesity-related insulin resistance. J Clin Invest *112*, 1821-1830.
Xu, M., Pirtskhalava, T., Farr, J.N., Weigand, B.M., Palmer, A.K., Weivoda, M.M., Inman, C.L., Ogrodnik, M.B., Hachfeld, C.M., Fraser, D.G., *et al.* (2018). Senolytics improve physical function and increase lifespan in old age. Nat Med *24*, 1246-1256.
Xu, X., Grijalva, A., Skowronski, A., van Eijk, M., Serlie, M.J., and Ferrante, A.W., Jr. (2013). Obesity activates a program of lysosomal-dependent lipid metabolism in adipose tissue macrophages independently of classic activation. Cell Metab *18*, 816-830.

Yoshino, J., Baur, J.A., and Imai, S.I. (2018). NAD(+) Intermediates: The Biology and Therapeutic Potential of NMN and NR. Cell Metab *27*, 513-528.
Yoshino, J., Mills, K.F., Yoon, M.J., and Imai, S. (2011). Nicotinamide mononucleotide, a key NAD(+) intermediate, treats the pathophysiology of diet- and age-induced diabetes in mice. Cell Metab *14*, 528-536.
Yoshizaki, T., Schenk, S., Imamura, T., Babendure, J.L., Sonoda, N., Bae, E.J., Oh, D.Y., Lu, M., Milne, J.C., Westphal, C*., et al.* (2010). SIRT1 inhibits inflammatory pathways in macrophages and modulates insulin sensitivity. Am J Physiol Endocrinol Metab *298*, E419-428.
Zhao, Y.J., Lam, C.M., and Lee, H.C. (2012). The membrane-bound enzyme CD38 exists in two opposing orientations. Sci Signal *5*, ra67.

Figure legends:

Figure 1. NAD decline during aging is associated with increased CD38+ tissue resident macrophages in eWAT.
(A) LC-MS was used to quantify NAD and NADP in whole visceral epididymal white adipose tissue (eWAT) from 6-month and 25-month-old mice. NAD and NADP concentrations are shown as pmol/mg of tissue.
(B) Flow cytometry gating strategy to identify resident and non-resident macrophages isolated from the stromal vascular fraction of eWAT, showing representative flow plots and histograms for the indicated age of mice.
(C). Quantification of total macrophages, CD38+ resident macrophages, and CD38+ non-resident macrophages isolated from eWAT of mice for the indicated age.
Data from individual mice are shown for *in vivo* experiments. Data is showing the mean ± SEM. Statistical significance defined as **P*<0.05, ***P*<0.01, and ****P*<0.00; two-sided Student's t-test except for 1A one-sided t-test was used.

Figure 2. M1 macrophages are characterized by increased NADase activity.
(A) NADase rates were measured in cell lysates from naive BMDMs (M0) or BMDMs treated with IL-4 (M2) or LPS (M1) after 16 hours of activation.
(B) Quantification of the NADase activity rate.
(C) LC-MS was used to quantify NAD and NAD related metabolites in naïve M0, M1, and M2, BMDMs for the indicated times.
(D) NAD/NAM ratios from LC-MS data above for each indicated time point
(E) mRNA expression of NAD consuming enzymes and NAD biosynthetic enzymes was measured using qPCR in untreated BMDMs (M0) or BMDMs polarized to the M1 and M2 state for the indicated times.
(F) Schematic representation of the NAM salvage pathway.
(G) NAD levels were measured by LC-MS in M0, M1 and M2 BMDMs pre-treated with or without 10nM/ml FK866 for 6 hours prior to stimulation with LPS for 6 hours or IL-4 for 16 hours.
Data is showing the mean ± SEM. (n=3 biological replicates). Statistical significance defined as **P*<0.05, ***P*<0.01, and ****P*<0.00; two-sided Student's t-test.

Figure 3. NAD levels regulate macrophage polarization.
(A) mRNA levels for M2 markers in BMDMs pre-treated with or without FK866 and NMN for 6 hours prior to stimulation with IL-4 for 16 hours.

(B) Arginase assay of M2 macrophages pre-treated with or without FK866 and NMN for 6 hours prior to stimulation with IL-4 for 16 hours.
(C-D) mRNA levels and ELISA measurements of TNF-α and IL-6 in supernatants from BMDMs pre-treated with or without FK866 and NMN for 6 hours prior to stimulation with LPS for 6 hours.
(E) Quantification of the half maximal effective concentration (EC_{50}) for NMN used to rescue M1 and M2 macrophage gene expression.
Data is showing the mean ± SEM. (n=3 biological replicates). Statistical significance defined as **P*<0.05, ***P*<0.01, and ****P*<0.00; two-sided Student's t-test. All statistical comparisons are relative to M2/M1 + FK866.

Figure 4. High NADase activity in M1 macrophages is CD38 dependent.
(A) Representative flow cytometry plots comparing CD38 surface staining in naive (M0) WT and *Cd38 KO* BMDMs or treated with IL-4 (M2) and LPS (M1) for 16 hours.
(B) NADase activity rates measured in WT and *Cd38 KO* MO, M2, and M1 BMDMs activated for 16 hours.
(C) Quantification of the NADase activity rate
(D) LC-MS was used to quantify NAD and NAD related metabolites in M0, M2, and M1 WT and *Cd38 KO* BMDMs activated for 16 hours.
(E) NAD/NAM ratios from LC-MS data above
Data is showing the mean ± SEM. (n=3 biological replicates). Statistical significance defined as **P*<0.05, ***P*<0.01, and ****P*<0.00; two-sided Student's t-test. Unless noted with a bar, all statistical comparisons are relative to untreated WT or *Cd38* KO sample.

Figure 5. Senescent cells promote CD38 expression in macrophages.
(A) mRNA levels of senescence markers, inflammatory genes, macrophage marker *Cd68*, and M2 genes in whole eWAT from 6-month and 25-month-old mice.
(B) mRNA levels in eWAT from 6-month-old mice IP injected with PBS or doxorubicin. Doxorubicin increases the expression of senescence markers, inflammatory cytokines, macrophage marker *Cd68* and *Cd38* in total tissue and in isolated macrophages.
(C) Flow cytometry analysis and quantification of CD38+ macrophages isolated from 6-month-old mice IP injected with PBS or doxorubicin.
(D) mRNA levels of *Cd38* in BMDMs treated with conditioned media from mouse dermal fibroblasts (MDF-CM), doxorubicin treated MDFs (Doxo MDF-CM), or irradiated MDFs (IRR MDF-CM) as described for 24 hours.
(E) mRNA levels of *Cd38* in BMDMs treated with the indicated TLR ligands for 16 hours.
(F) mRNA levels of *Cd38* in BMDMs treated with the indicated DAMP ligands for 16 hours.
(G) mRNA levels of inflammatory genes in MDFs and IRR-MDFs.
(H) mRNA levels of *Cd38* in BMDMs treated with the indicated concentration (ng/ml) of recombinant mouse cytokines for 24 hours.
(I) Flow cytometry of Edu+ BMDMs treated with MDF-CM or IRR MDF-CM for 24 hours.
(J) Bright field microscopy image of BMDMs treated with MDF-CM or IRR MDF-CM for 24 hours
For *in vivo* experiments, data from individual mice are shown.
Data is showing the mean ± SEM. (n=3 biological replicates except n=4 in G). Statistical significance defined as **P*<0.05, ***P*<0.01, and ****P*<0.00; two-sided Student's t-test except for 5a and 5b one-tailed t-test was used.

Figure 6. Proposed model how aging-related inflammation leads to enhanced NAD degradation. Aging is associated with the accumulation of DNA damage, which leads to genotoxic stress and the slow accumulation of senescent cells over time. Using in vivo and in vitro senescent cell model systems, we show that the accumulation of senescent cells and the

accompanying inflammatory cytokines of the senescence-associated secretory phenotype (SASP) is sufficient to promote CD38 expression and macrophage proliferation. In addition, increased intestinal permeability has been reported to occur during aging leading to enhanced serum levels of endotoxins and other pathogen-associated molecular patterns (PAMPs) which can activate the PRRs expressed by innate immune cells. Collectively, SASP and PAMPs can promote an inflammatory state associated with increased expression of CD38 by tissue resident M1-like macrophages characterized by enhanced NADase activity. In addition, we show that NAD is a critical regulator of macrophage polarization, and that NAD fine-tunes a subset of genes expressed during the anti-inflammatory M2 program. Thus, our data suggest that during aging a subset of M2 macrophage genes may be affected as NAD levels decline.

Materials and Methods:

Mice: C57BL/6J mice were used for *in vivo* studies and as a source of BMDMs. Mice were maintained at Buck Institute on a standard chow diet and all procedures were performed in accordance with the guidelines set forth by the Institutional Animal Care and Use Committees (IACUC) at the institution. *Cd38 KO* mice on a C57BL/6J background were obtained from The Jackson Laboratory (Bar Harbor, ME) and were bred and housed at our animal facility at the Gladstone Institute and Buck Institute.

BMDM culture and experiments: BMDMs used in experiments were derived from bone marrow extracted from the femurs of euthanized mice (6-12 weeks old male and female C57BL/6J) by mortar and pestle. Briefly, femurs, were placed in the mortar and were washed with 70% ethanol to sterilize followed by two washes with complete RPMI (cRPMI; standard RMPI (Corning) supplemented with 10% fetal calf serum, penicillin-streptomycin solution (Corning), 1mM sodium pyruvate solution (Corning), 2mM L-Glutamine solution (Corning), 10nM HEPES buffer (Corning), and 50μM 2-mercaptoethanol). After washing, 10mls of cRPMI were added to the mortar and the femur bones were gently crushed. The resulting media was collected and filtered through a 70μm filter and placed in a conical tube. The filtered supernatant was centrifuged at 1200 RPM (150 RCF) for 5 minutes. Cells were resuspended, counted and plated at a density of $3x10^6$ cells/10cm dish in 10ml of macrophage growth media (cRPMI containing 25% M-CSF containing L929 conditioned media (made in house)). Cells were left to grow for 7 days to differentiate and were supplemented with 5ml of macrophage growth media on day 5. On day 7, BMDMs (yielding $10\text{-}12x10^6$ cells/10cm dish) were lifted off the plate using cold PBS containing 5mM EDTA. BMDMs were counted and replated in macrophage growth media overnight prior to experiments. On day of experiments, macrophage growth media was replaced with cRPMI 6 hours prior to stimulation to remove M-CSF. M2 polarization was performed by stimulating macrophages with 10ng/ml recombinant mouse IL-4 (Peprotech). For M1 polarization macrophages were stimulated with 100ng/ml LPS (LPS EK-Ultrapure, Invivogen). To test how different TLR ligands activate CD38, a Mouse TLR Agonist kit was purchased from Invivogen and BMDMs were treated with each ligand for 16 hours.

Gene expression measurement: For *in vitro* experiments RNA was isolated using RNA STAT 60 (Amsbio) per manufacturer's protocol. 1µg RNA was converted to cDNA using a High Capacity cDNA Reverse Transcription Kit (Applied Biosystems), and diluted with 280µl H_2O post reaction. Gene expression was measured using a CFX384 Real Time System (Bio-Rad) and Thermo Scientific Maxima 2x SYBR Green. Data was analyzed using the CFX Bio-Rad software and normalized using the delta/delta CT method. In vitro BMDMs were normalized to the housekeeping gene hypoxanthine phosphoribosyltransferase (*Hprt*). For in vivo experiments RNA was extracted from flash frozen epididymal fat samples using Trizol (ThermoFisher) in a TissueLyser system (Qiagen). cDNA was generated as described above and gene expression was measured in a LightCycler480 II using the Universal Probe Library system (Roche). Expression was normalized to *Actin* and *Tubulin* using the delta/delta CT method.

***In vivo* experiments**

Male C57BL/6J mice were obtained from the National Institute on Aging colony and The Jackson Laboratory (Bar Harbor, ME). Mice ranging in age from 2 to 30-months old were used for determination of the effects of natural aging. 6-months old mice were injected intraperitoneally with a single dose of 10 mg doxorubicin/kg or vehicle (PBS) and euthanized six weeks later. All animals were euthanized by CO_2 followed by cervical dislocation. Epididymal fat was excised and portions of the tissue were either flash frozen in liquid nitrogen for qPCR analysis or processed for flow cytometry as described below. All procedures were approved by the Buck Institute IACUC and were in compliance with approved animal protocols.

NAD Metabolome Mass Spectrometry: For adipose tissue NAD and NADP levels, fat samples were received on dry ice and stored at -80 °C. Samples were pulverized prior to extraction by freezing in LN_2 and adding to a Bessman pulverizer cooled to LN_2 temperature. Samples were weighed frozen into microcentrifuge tubes cooled to LN_2 temperature. The appropriate internal standard solution was added and the sample extracted with hot 75%Ethanol/25% HEPES (pH 7.1) buffer as previously described (Trammell and Brenner, 2013). After centrifugation, the aqueous layer between the cell pellet and lipid layer was withdrawn and transferred to a clean microcentrifuge tube; the solvent was evaporated to dryness using a vacuum centrifuge. Standards and controls were prepared by adding internal standard, the appropriate amount of standard working solution, and ethanol/HEPES buffer to microcentrifuge tubes; the standards were dried along with the samples. The dried samples were stored at -20°C until reconstitution immediately prior to the analytical run. For analysis, samples were reconstituted in 70µL of 10mM ammonium acetate and analyzed using 2 separations as previously described(Trammell and Brenner, 2013; Trammell et al., 2016), and tissue NAD and NADP levels were normalized to tissue weight. Cells Methodology**:** Briefly, $7x10^6$ BMDMs were cultured in 10cM TC-plates overnight in macrophage growth medium to ~90% confluence. The following day, the media was replaced with cRPMI 6hrs prior to stimulating with IL-4 (10ng/ml) or LPS (100ng/ml) for the indicated timepoints. BMDMs were washed twice with cold PBS, and gently scraped off, counted, pelleted, flash frozen, and shipped overnight on dry ice to the Brenner Lab. Cell pellets of BMDMs were received on dry ice and stored at -80 °C. To extract metabolites the appropriate internal standard was added along with 400µL of hot ethanol/HEPES buffer as described previously.[1] Calibrators and controls were prepared and solvent removed in a vacuum

centrifuge. The analytical runs were conducted as above. BMDM metabolite levels were normalized to cell number (pmol/1x10^6 cells) and graphed as normalized peak area. Internal standards**:** Stable isotope analogs of nucleotides and nucleoside were grown in a yeast broth with universally labelled ^{13}C glucose, resulting in all ribose rings being fully labelled. $^{13}C_{10}$ NAD was used as its internal standard. For the second analysis a mix of ^{18}O-NR, ^{18}O-Nam, d_4-NA, d_3-MeNam, and d_3- methyl-4-pyridone-3-carboxamide was used as internal standard.

Quantification of tryptophan and metabolites levels: Quantification was performed as previously described (Huang et al., 2013). Briefly, 7x10^6 BMDMs were cultured in 10cM TC-plates overnight in macrophage growth medium to ~90% confluence. The following day, the media was replaced with cRPMI 6hrs prior to stimulating with IL-4 (10ng/ml) or LPS (100ng/ml) for 24hrs. Cells were washed twice with cold PBS, and gently scraped off, pelleted, flash frozen, and shipped to the Lee lab on dry ice. The extracted tryptophan and metabolites analyzed by LC-ESI-MS/MS (API 5000 QTRAP mass, AB/SCIEX) by MRM mode. The tryptophan and metabolites MS/MS transitions (*m*/*z*) were 205→188 for tryptophan, 209→192 for kynurenine, 225→208 for 3-hydroxy-L-kynurenine, 154→136 for 3-hydroxyanthranilic acid, 206→160 for kynurenic acid, 190→144 for xanthurenic acid, 138→120 for anthranilic acid, 124→106 for 2-picolinic acid, 168→150 for quinolinic acid, and 199→112 for L-mimosine as an internal standard, respectively. The metabolites were separated on a Luna C18 column (2.1 × 150 mm, 5.0μm) with an injection volume of 5μL and a flow rate of 0.3 ml/min using 0.1% trifluoroacetic acid for mobile phase A and acetonitrile for mobile phase B. The gradient was as follows: 0 min, 2% B; 12 min, 60% B; 13 min, 60% B; 14 min, 2% B; 20 min, 2% B. Data were acquired using Analyst 1.5.1 software (Applied Biosystems, Foster City, CA). Data is presented as pmol/mg protein.

Extraction of nicotinamide riboside (NR) and analysis by LC-MS/MS.
To define the relative abundance of NR by LC-MS/MS analyses, a previously described extraction method optimized for NAD, NADP and NADPH was employed (Lewis et al., 2014). Briefly, 7x10^6 BMDMs were cultured in 10cM TC-plates overnight in macrophage growth medium to ~90% confluence. The following day, the media was replaced with cRPMI 6hrs prior to stimulating with LPS (100ng/ml) for the indicated timepoints. Cells were washed twice with cold PBS, and gently scraped off, pelleted, flash frozen, and shipped overnight to the Ben-Sahra Lab on dry ice. Metabolites were extracted on ice with 250μl of a 40:40:20 mixture of Acetonitrile/Methanol/ (10mM Tris, pH 9.2, 200mM NaCl). Supernatants were stored at -80°C (one week or less) and 25μl of the cleared solution was injected in a Thermo Q-Exactive (LC-MS) in line with an electrospray source and an Ultimate3000 (Thermo) series HPLC consisting of a binary pump, degasser, and auto-sampler outfitted with a Xbridge Amide column (Waters; dimensions of 4.6mm × 100mm and a 3.5μm particle size). The mobile phase A contained 95% (vol/vol) water, 5% (vol/vol) acetonitrile, 20mM ammonium hydroxide, 20mM ammonium acetate, pH 9.0; B was 100% Acetonitrile. The gradient was as follows: 0 min, 15% A; 2.5 min, 30% A; 7 min, 43% A; 16 min, 62% A; 16-18 min, 75% A; 18-25 min, 15% A with a flow rate of 400μl/min. The capillary of the ESI source was set to 275°C, with sheath gas at 45 arbitrary units, auxiliary gas at 5 arbitrary units and the spray voltage at 4.0 kV. In positive/negative polarity switching mode, an m/z scan range from 70 to 850 was chosen and MS1 data was

collected at a resolution of 70,000. The automatic gain control (AGC) target was set at 1×10^6 and the maximum injection time was 200ms. The top 5 precursor ions were subsequently fragmented, in a data-dependent manner, using the higher energy collisional dissociation (HCD) cell set to 30% normalized collision energy in MS2 at a resolution power of 17,500. The sample volumes of 25µl were injected. Data acquisition and analysis were carried out by Xcalibur 4.0 software and Tracefinder 2.1 software, respectively (both from ThermoFisher Scientific). NR peak area was normalized to protein concentration for each sample and graphed as normalized peak area. Metabolomics services were performed by the Metabolomics Core Facility at Robert H. Lurie Comprehensive Cancer Center of Northwestern University.

Adipose tissue Digestion: Adipose tissue digestion was performed as previously described (Covarrubias et al., 2016). Briefly, adipose tissue was excised and minced, prior to being digested with 2mg/ml collagenase (Sigma) diluted with KRBH containing 2% FBS for 30 minutes at 37℃. The resulting suspension was filtered through a 70µm filter and centrifuged for 5 minutes at 2000 RPM (425 RCF). The fat layer and supernatant were discarded, and the cell pellet (SVF) was then washed twice with PBS containing 1mM EDTA and 2% FBS prior to lysing red blood cells with ACK lysis buffer (made in house) and staining cells with antibodies for flow cytometry as described below.

Flow Cytometry: Isolated adipose tissue stromal vascular cells (SVF), cleared of red blood cells using ACK lysis buffer (as described above), were counted and blocked with anti-mouse FC-block (BD Biosciences) per manufacturer's protocol for 15 minutes on ice. Cells were subsequently labelled on ice for 30 minutes with the following antibodies diluted 1:200; CD38-FITC (clone 90, Biolegend), CD11c-APC (N418, Biolegend), CD11b-PECy7 (M1/70, eBioscience), CD45.2 PE (clone 104, eBioscience), and F4/80-BV510 (clone BM8, Biolegend). Cells were immediately analyzed using the BD FACSAria flow cytometer. Compensation and analysis of the data was performed using the FlowJo software. For in vitro experiments activated BMDMs were lifted off of non-TC treated cell tissue plates after activation using cold PBS with 5mM EDTA for 15 minutes prior to blocking with FC block and staining with antibodies using the protocol described above. Click-iT EdU 488 Flow Cytometry Kit (ThermoFisher) was used to measure macrophage proliferation per manufacturers protocol.

Human PBMC Macrophage Experiment:
Peripheral blood mononuclear cells (PBMCs) were purified from healthy donor blood (Blood Centers of the Pacific, San Francisco, CA) from continuous-flow centrifugation leukophoresis product using density centrifugation on a Ficoll-Paque gradient (GE Healthcare Life Sciences, Chicago, IL). Monocyte were isolated by adherence: 3×10^6 PBMC were seeded into 10cm cell culture dishes and allowed to adhere in a 5% CO_2 incubator at 37˚C for 2-3 hours in cRPMI. Non-adherent cells were removed and the adherent cells were carefully washed, twice with PBS. For the generation of human macrophages, monocytes isolated by adherence were cultured in complete RPMI supplemented with 100ng/ml recombinant human M-CSF (Peprotech) in a 5% CO_2 at 37˚C for 7 days. After 7 days, the cells were stimulated with 100ng/ml LPS or 10ng/ml recombinant human IL-4 for 18 hours.

ELISA: TNF−α and IL-6 were measured in the media of activated BMDMs using ELISA kits purchased from Biolegend per manufacturer's protocol. Prior to ELISA supernatants were cleared of debris or dead cells by centrifuging for 5 minutes at 425RCFx5min and diluted 1:150 with the ELISA dilution buffer recommended in the kit.

Western Blot: Cell lysates were prepared by lysing cells with RIPA Buffer containing Halt protease and phosphatase inhibitor cocktail (ThermoFisher). Protein concentrations were determined using BCA Assay kit (ThermoFisher). Approximately, 15µg of protein lysates were loaded onto 8% polyacrylamide gels and transferred to PVDF membranes. The following primary antibodies were purchased from Cell Signaling and were used to probe for proteins; Tubulin (9F3), Parp1 (46D11), Sirt1 (1F3).

Arginase Assay: Arginase Assay was performed as previously described (Byles et al., 2013). Briefly, 0.5 x10^6 stimulated BMDMs were lysed with 75µl 0.1% TritonX-100 lysis buffer with Halt protease inhibitor cocktail (ThermoFisher). Lysate arginine was activated by adding 50µl of 25mM Tris-HCL and 10µl of 2mM $MnCl_2$ to each sample and heating at 56°C for 10 minutes. 100µl of 500mM L-Arginine (pH 9.7) was added to each tube and left to incubate 45 minutes at 37°C. 800µl acid solution (H_2SO_4: H_3PO_4: H_2O (1:3:7)) was used to stop each reaction. Urea production was measured by adding 40µl of 9% a-isonitrosopropiophenone (dissolved in 100% ethanol) to each sample and heated to 100°C for 15 minutes. A standard curve of urea was run in parallel to the samples and standards/samples were measured at 540nm using a plate reader.

NADase Assay: NADase activity was measured using a fluorescence-based assay. Briefly, 0.5 × 10^6 BMDMs/sample were lysed with 0.1% TritonX-100 Sucrose-Tris (0.25 M sucrose, 40mM Tris [pH 7.4]) lysis buffer with protease and phosphatase inhibitors (ThermoFisher). For the NADase assay on intact macrophages, 2.5 × 10^6 BMDMs/sample were gently lifted with the cell scraper, centrifuged and resuspended in 100µl PBS/well. The reaction was started adding 80µM of nicotinamide 1,N^6-etheno-adenine dinucleotide (Sigma Aldrich). The samples were excited at 340 nm and the emission of fluorescence was measured at 460nm at 37°C every min for 1hr in a PHERAstar FS microplate reader (BMG LABTECH). NADase activity was calculated as the slope of the linear portion of the fluorescence-time curve, corrected by the amount of protein in each sample. Protein concentrations were determined using BCA Assay kit (ThermoFisher).

Senescence Cell Condition Media Experiment: Irradiation induced senescence, mouse dermal fibroblasts (MDF) were exposed to 10Gy X-rays and medium was changed to fresh medium every 2 days. Control cells were mock irradiated. For chemotherapy-induced senescence MDF were treated with doxorubicin (Sigma Aldrich) at concentration 250nM in DMSO for 24 hr. The medium was replaced by normal DMEM supplemented with 10% FBS and refreshed every 2 days. Control cells were treated with equal amount of DMSO. After day 10 of treatment, conditioned medium (CM) were prepared by washing cells 3 times in PBS, then incubating in media for 24 h. Bone marrow derived macrophages then incubated with this CM for 24 hours and harvested for RNA isolation. For co-culture experiments, 1x10^6 WT or *Cd38 KO* BMDMs were counted and added to 6-well tissue culture plates containing 1x10^4 IRR MDFs

or control MDFs at a ratio of (10:1) in 3.5mls of DMEM supplemented with 10% FBS in a 6-well plate for 24 hours. Co-culture cells were harvested with RNA Stat 60 to analyze gene expression of bulk RNA from both macrophages and senescent cells as described above.

Statistical Analysis: Statistical analysis was performed using GraphPad Prism software and Microsoft Excel. One-sided and two-sided Student's t-tests were applied to comparisons between two conditions with mean ± SEM shown. NS, not significant, *P<0.05, **P<0.01, and ***P<0.001.

Figure 1

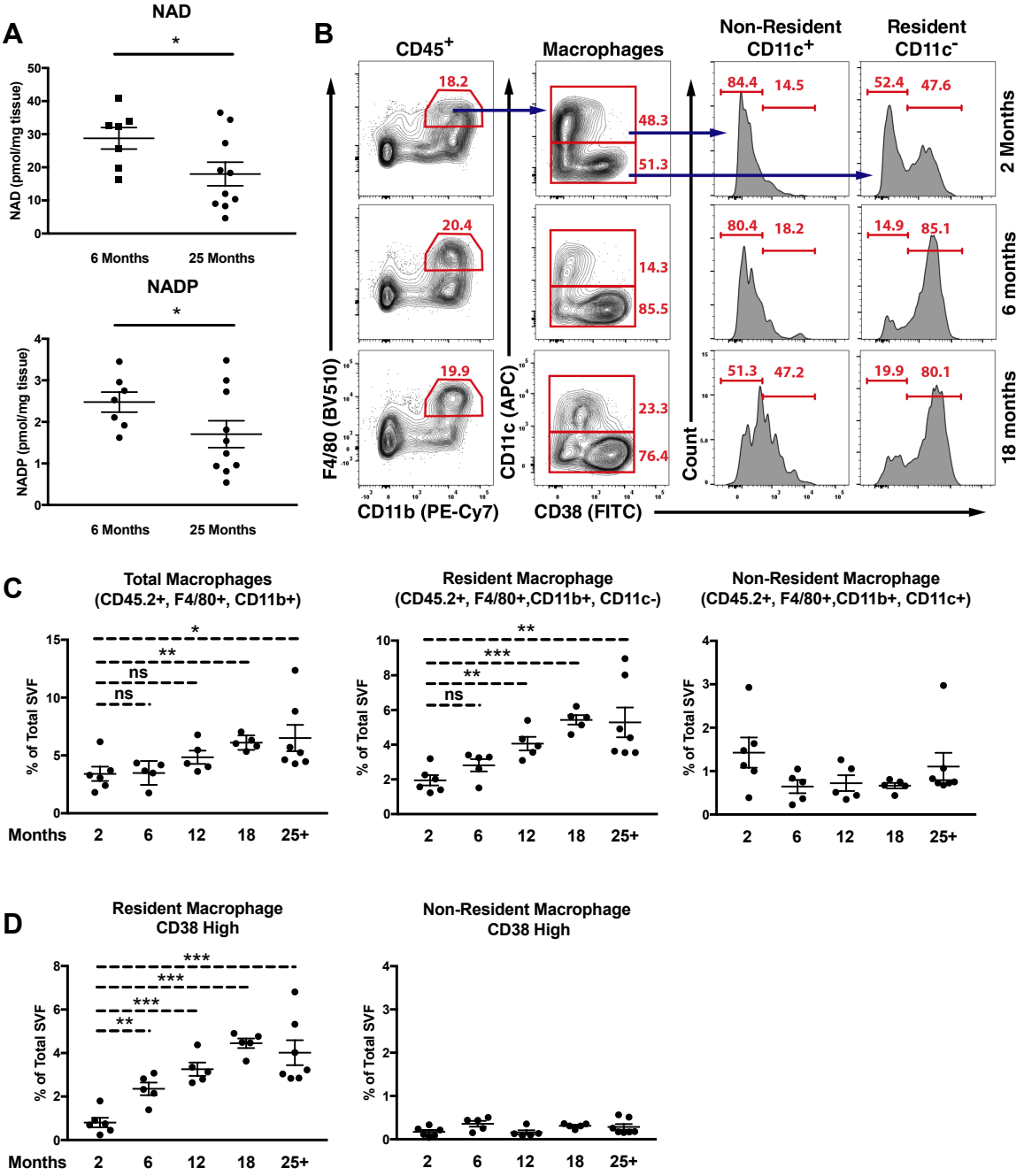
A
NAD
*
NAD (pmol/mg tissue)
50
40
30
20
10
0
6 Months
25 Months
NADP
*
NADP (pmol/mg tissue)
4
3
2
1
0
6 Months
25 Months
B
CD45+
Macrophages
Non-Resident CD11c+
Resident CD11c-
18.2
48.3
51.3
84.4
14.5
52.4
47.6
2 Months
20.4
14.3
85.5
80.4
18.2
14.9
85.1
6 months
19.9
23.3
76.4
51.3
47.2
19.9
80.1
18 months
F4/80 (BV510)
CD11b (PE-Cy7)
CD11c (APC)
CD38 (FITC)
Count
C
Total Macrophages
(CD45.2+, F4/80+, CD11b+)
Resident Macrophage
(CD45.2+, F4/80+,CD11b+, CD11c-)
Non-Resident Macrophage
(CD45.2+, F4/80+,CD11b+, CD11c+)
% of Total SVF
*
**
ns
***
Months
2
6
12
18
25+
D
Resident Macrophage
CD38 High
Non-Resident Macrophage
CD38 High
% of Total SVF
***
**
Months
2
6
12
18
25+

Figure 2

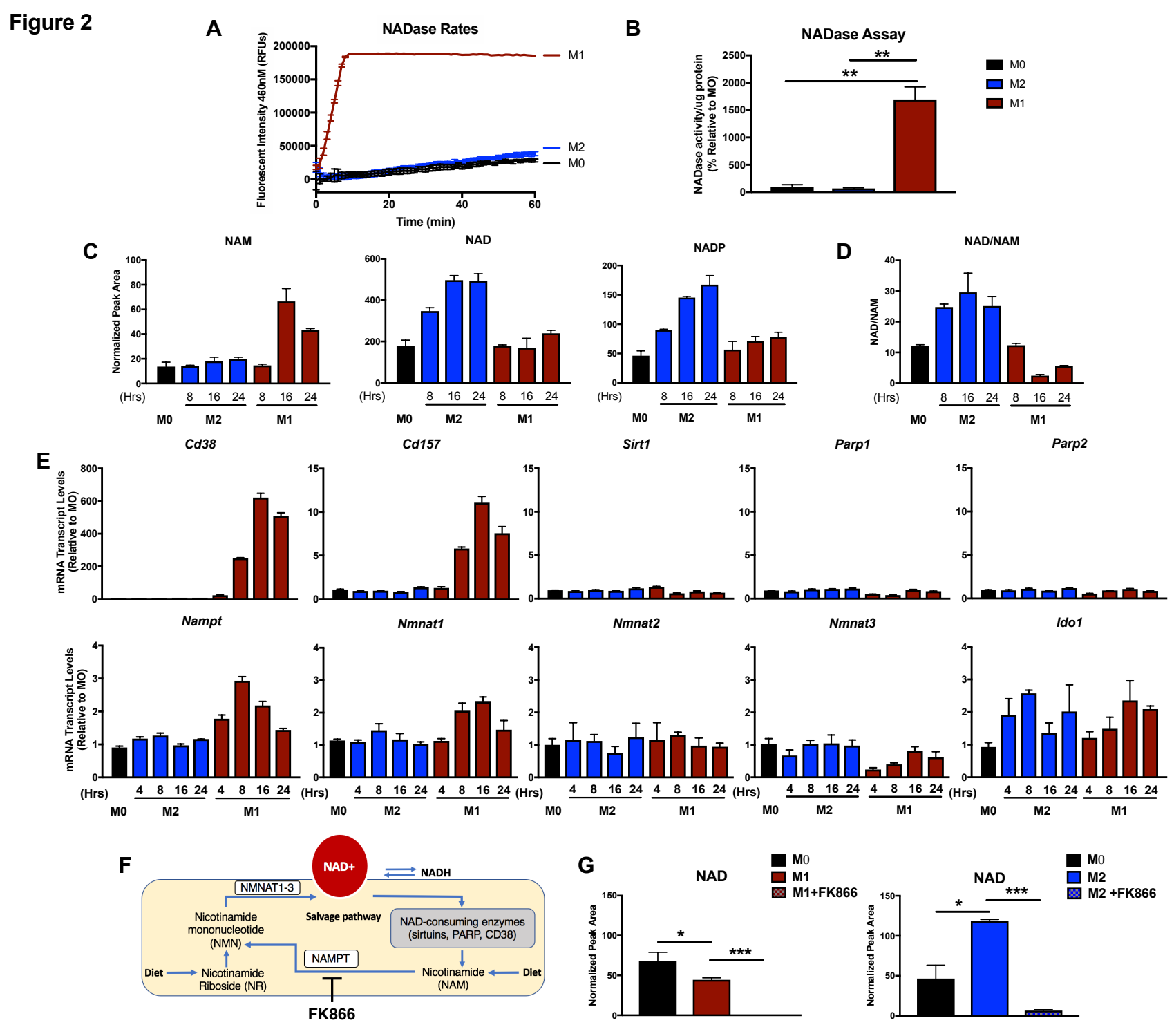
A
NADase Rates
Fluorescent Intensity 460nM (RFUs)
Time (min)
M1
M2
M0
B
NADase Assay
NADase activity/ug protein (% Relative to M0)
M0
M2
M1
C
NAM
NAD
NADP
Normalized Peak Area
(Hrs)
M0
M2
M1
D
NAD/NAM
E
Cd38
Cd157
Sirt1
Parp1
Parp2
Nampt
Nmnat1
Nmnat2
Nmnat3
Ido1
mRNA Transcript Levels (Relative to M0)
F
NAD+
NADH
NMNAT1-3
Salvage pathway
Nicotinamide mononucleotide (NMN)
NAD-consuming enzymes (sirtuins, PARP, CD38)
NAMPT
Diet
Nicotinamide Riboside (NR)
Nicotinamide (NAM)
FK866
G
NAD
M0
M1
M1+FK866
M2
M2 +FK866
Normalized Peak Area

Figure 3

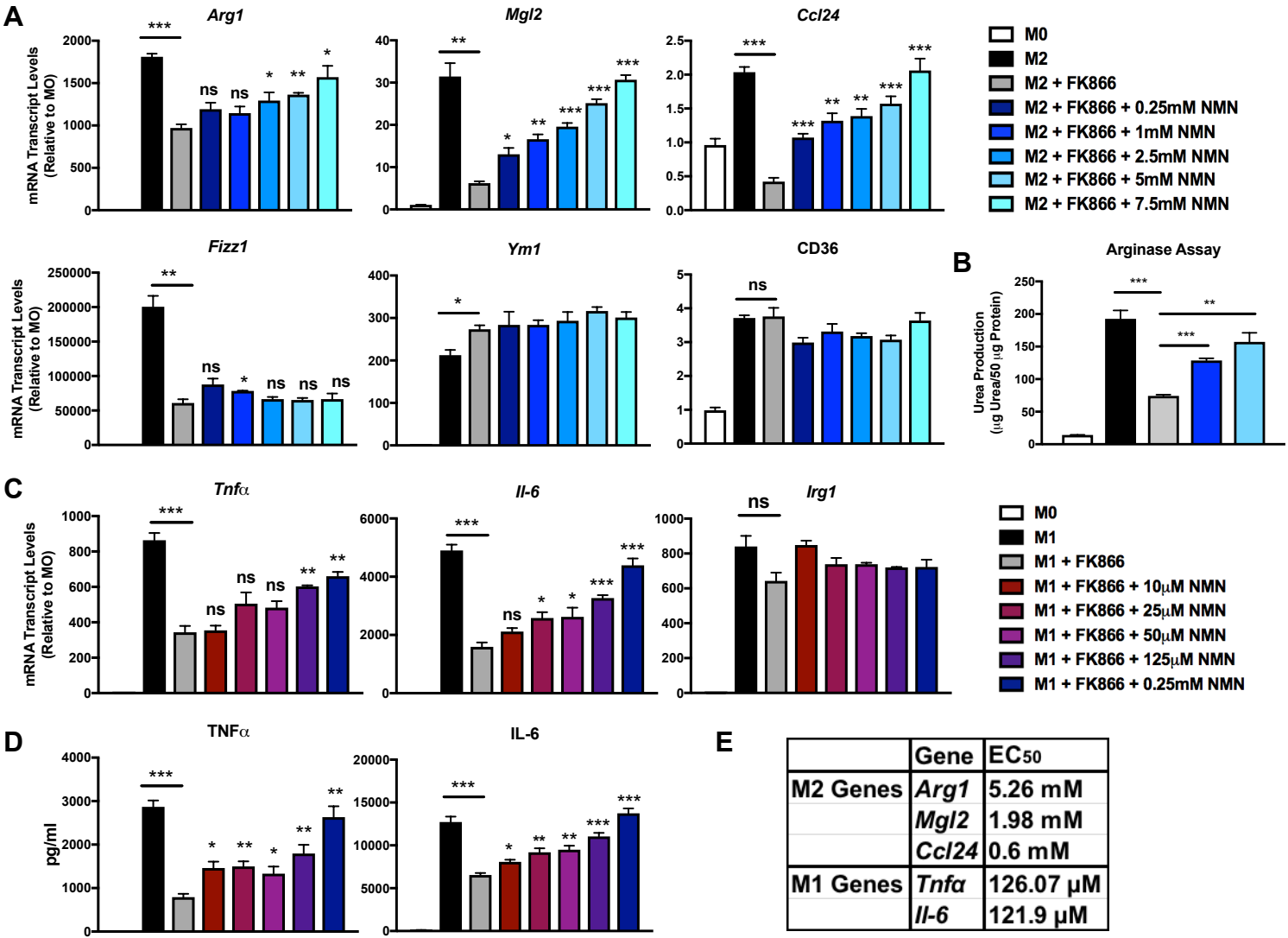

	Gene	EC_{50}
M2 Genes	*Arg1*	5.26 mM
	Mgl2	1.98 mM
	Ccl24	0.6 mM
M1 Genes	*Tnfα*	126.07 μM
	Il-6	121.9 μM

Figure 4

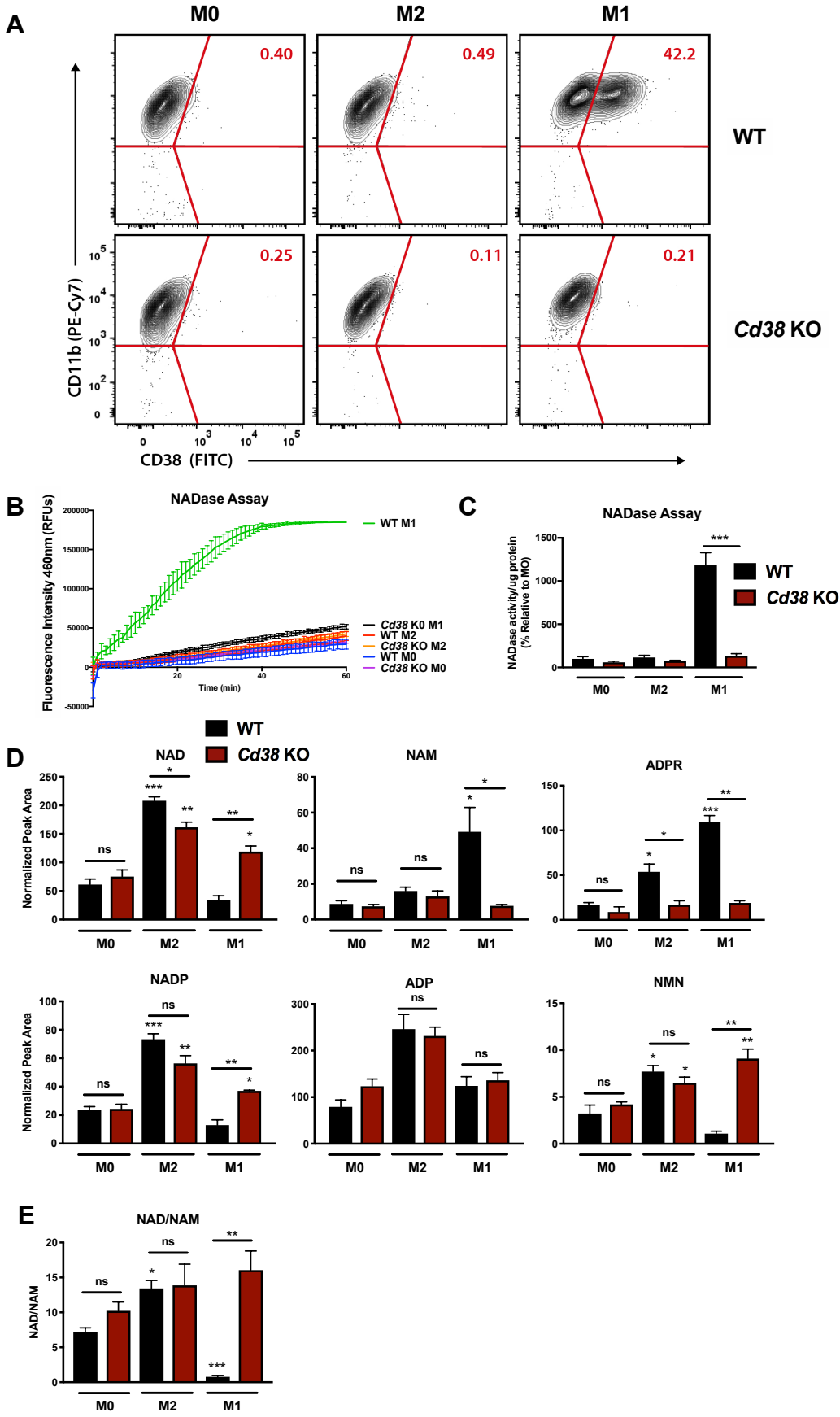
A
M0
M2
M1
0.40
0.49
42.2
WT
0.25
0.11
0.21
Cd38 KO
CD11b (PE-Cy7)
CD38 (FITC)
B
NADase Assay
Fluorescence Intensity 460nm (RFUs)
Time (min)
WT M1
Cd38 KO M1
WT M2
Cd38 KO M2
WT M0
Cd38 KO M0
C
NADase Assay
NADase activity/ug protein (% Relative to M0)
WT
Cd38 KO
D
WT
Cd38 KO
NAD
NAM
ADPR
NADP
ADP
NMN
Normalized Peak Area
E
NAD/NAM

Figure 5

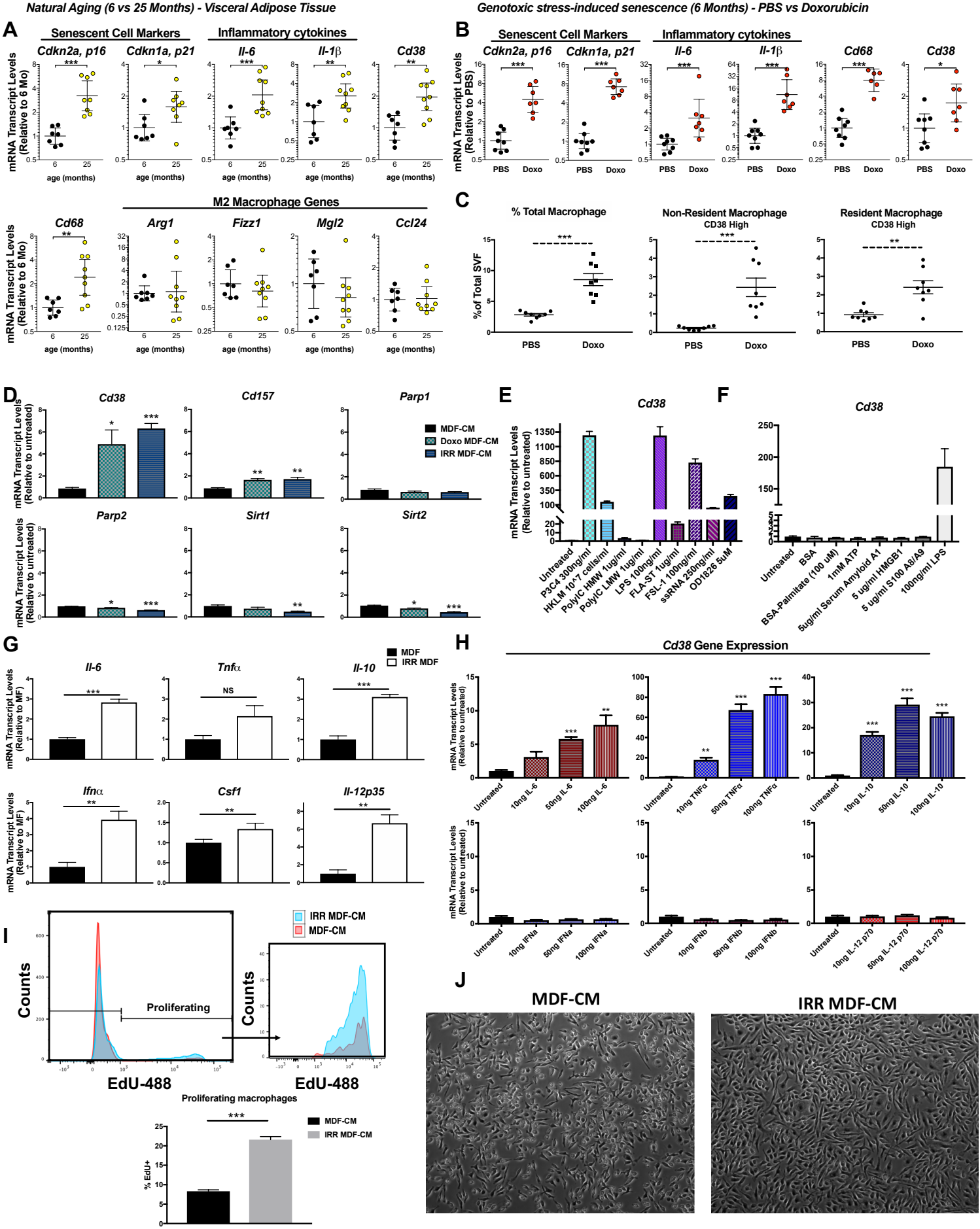
Natural Aging (6 vs 25 Months) - Visceral Adipose Tissue
Genotoxic stress-induced senescence (6 Months) - PBS vs Doxorubicin
A
Senescent Cell Markers
Inflammatory cytokines
Cdkn2a, p16
Cdkn1a, p21
Il-6
Il-1β
Cd38
mRNA Transcript Levels (Relative to 6 Mo)
age (months)
M2 Macrophage Genes
Cd68
Arg1
Fizz1
Mgl2
Ccl24
B
mRNA Transcript Levels (Relative to PBS)
PBS
Doxo
C
% Total Macrophage
%of Total SVF
Non-Resident Macrophage
CD38 High
Resident Macrophage
CD38 High
D
Cd38
Cd157
Parp1
Parp2
Sirt1
Sirt2
mRNA Transcript Levels (Relative to untreated)
MDF-CM
Doxo MDF-CM
IRR MDF-CM
E
Cd38
mRNA Transcript Levels (Relative to untreated)
Untreated
P3C4 300ng/ml
HKLM 10^7 cells/ml
PolyIC HMW 1ug/ml
PolyIC LMW 1ug/ml
LPS 100ng/ml
FLA-ST 1ug/ml
FSL-1 100ng/ml
ssRNA 250ng/ml
OD1826 5uM
F
Cd38
Untreated
BSA
BSA-Palmitate (100 uM)
1mM ATP
5ug/ml Serum Amyloid A1
5 ug/ml HMGB1
5 ug/ml S100 A8/A9
100ng/ml LPS
G
MDF
IRR MDF
Il-6
Tnfα
Il-10
Ifnα
Csf1
Il-12p35
mRNA Transcript Levels (Relative to MF)
NS
H
Cd38 Gene Expression
mRNA Transcript Levels (Relative to untreated)
Untreated
10ng IL-6
50ng IL-6
100ng IL-6
10ng TNFα
50ng TNFα
100ng TNFα
10ng IL-10
50ng IL-10
100ng IL-10
10ng IFNa
50ng IFNa
100ng IFNa
10ng IFNb
50ng IFNb
100ng IFNb
10ng IL-12 p70
50ng IL-12 p70
100ng IL-12 p70
I
IRR MDF-CM
MDF-CM
Counts
Proliferating
EdU-488
Proliferating macrophages
% EdU+
J
MDF-CM
IRR MDF-CM

Figure 6

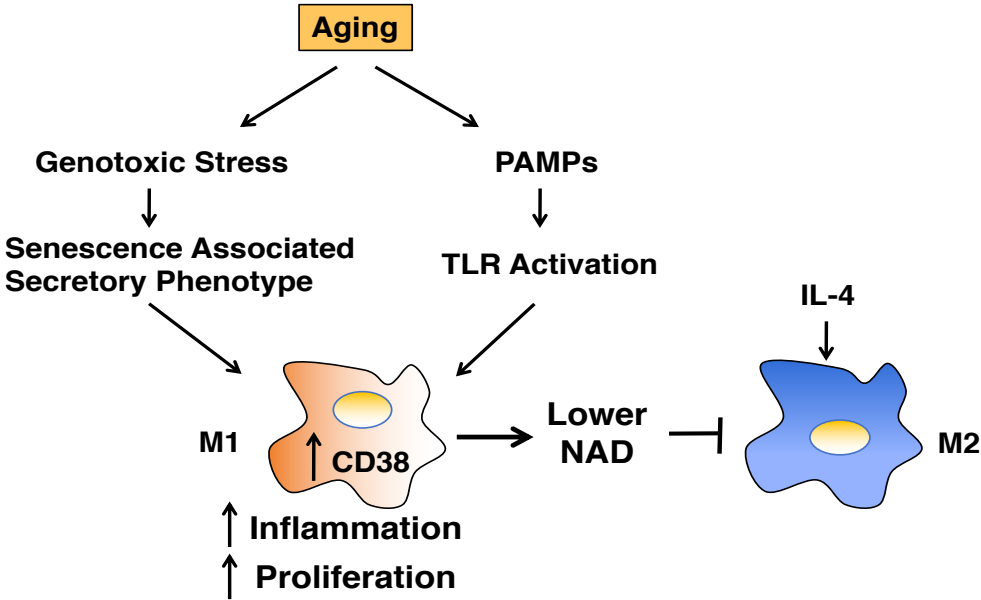
Aging
Genotoxic Stress
PAMPs
Senescence Associated
Secretory Phenotype
TLR Activation
IL-4
M1
CD38
Lower
NAD
M2
Inflammation
Proliferation